SUPERSONIC MOLECULAR BEAM STUDY OF THE DIRECT-INELASTIC SCATTERING AND THE TRAPPING-DESORPTION OF Br_2 ON GaAs (100)

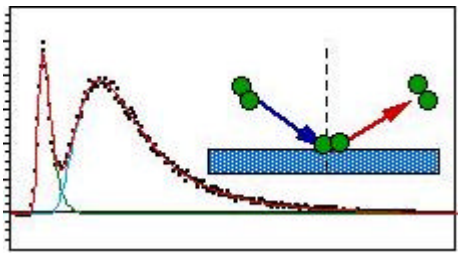

Molecular Beam Group
Chemistry Department
University of Manchester

By Jose L. Ibarra M.
Supervised by Peter A. Gorry

Index

Abstract

This report contains an account of the quantum descriptions of rotational, vibrational and electronic motions. It also provides an introduction to basic absorption and emission spectra, the Franck-Condon principle, fluorescence and laser action.
The apparatus used for the supersonic molecular beam scattering experiments is described. The results of a study of direct-inelastic scattering and trapping-desorption of Br_2 on GaAs (100) are presented.
Finally a description of the theoretical basis of Laser Induced Fluorescence, LIF, is presented with some early results.

At the beginning, I started with the bibliography supported by the group, Johnathan P. Essex-Lopresti's thesis and Steve Bullmann's thesis being very useful plus invaluable help from Dr. Weijie Jia.
Full descriptions of the Molecular Beam Scattering and time of flight techniques are found in the thesis of Jonathan Essex-Lopresti. Steve Bullmann's thesis contains details of the theory for Laser-Induced-Fluorescence (LIF). Also very helpful have been the explanations of Dr. Jia who has introduced me to both the apparatus and the theoretical basis of the experiments, answering important questions such as what do we do? How do we do it? And what is the theoretical basis for the work?

With the work in the laboratory we try to understand the physical mechanisms that govern gas-surface interactions. In our case, we develop theory and experiments applied to GaAs semiconductor for the fabrication of microchips. The production of the integrated circuits requires surface etching and deposition of other materials on to the surface to build the electronic components.
The techniques used for these studies are molecular beam scattering of halogen molecules on the surface, time of flight (TOF) mass spectrometry and laser induced fluorescence (LIF) to study direct-inelastic scattering and trapping-desorption.

Introduction [1,2,3,4,5]

The work described in this report is the Supersonic molecular beam study of the direct-inelastic scattering and trapping desorption of Br_2 and an introduction to the laser-induced fluorescence technique.
To understand the above it is necessary to give a description of some basic spectroscopy. We can define spectroscopy as branch of chemical or physical science that deals with the study of spectra. This is made up of two parts: experiment and theory. The experiment obtains the spectrum and measures it and theory extracts the information contained in the spectrum, such as the molecular structure of the molecule.
A spectrum is a graphical representation, fig. 1, of the distribution of the intensity of light absorbed or emitted from the sample as function of the wavelength or frequency of radiation.

Fig. 1

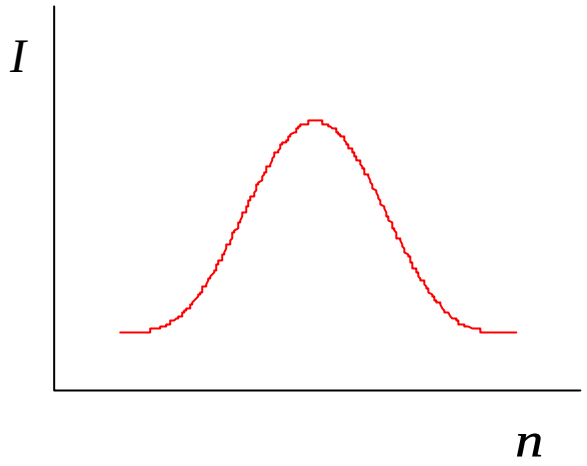

To obtain this, it is necessary to consider the interaction between the radiation and the sample. Spectra can be divided in emission spectra and absorption spectra. The first is obtained by exciting the sample, and then the sample emits radiation. For the second one, we illuminate the sample with continuous radiation and analyse the absorbed radiation as function of the wavelength. According to Bohr, electromagnetic radiation is not emitted while an electron moves in its orbit, but only when the electron goes from one quantum orbit of energy E_n to another of energy E_m. This process is called a quantum jump. The liberated energy E_n-E_m is emitted as a light quantum (photon) of energy $E_n - E_m = h\nu$ (ν = wave number of the light) and this is the *Bohr's frequency condition.* Then the wave number of the emitted or absorbed light is

$$\nu' = \frac{E_n - E_m}{hc} \qquad (1)$$

where $\nu' = \frac{\nu}{c}$

If $E_n < E_m$, radiation of this wave number is emitted by the system. The frequencies of the emitted or absorbed spectral lines are determined by the energy values of the system. The probabilities of the transitions under the influence of radiation are determined by the eigenfunctions of the states involves. Thus the intensities of the emitted or absorbed spectral lines can be obtained. And knowing the eigenfunctions, we can calculate whether or not two states can combine with each other.
A description of rotational, vibrational and electronic motion is essential to understand the work.

Quantization-Particle on a ring

As an example of quantization we start with the solution for a particle on ring using $E = \frac{p^2}{2m}$ then $E = \frac{L^2}{2I}$ because $L = pr$ and $I = mr^2$, L is the magnitude of the angular momentum, and if $p = \frac{h}{\lambda}$, then the angular momentum, l, is related to the wavelength of the particle's wavefunction. Suppose for the moment that λ can take an arbitrary value, then the wavefunction will vary around the ring as the angle ϕ increases, where ϕ is the angle that describes the ring, and its value is between 0 and 2π

It is necessary to find a solution where the wavelength is such that the wavefunction reproduces itself on successive circuits, fig 2:

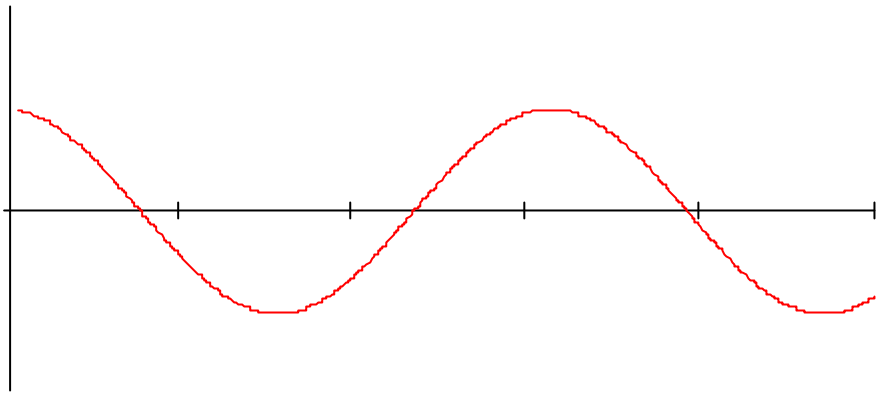

Then, only some angular momentum values are acceptable, hence:

$$\lambda = \frac{2\pi r}{n} \text{ with } n = 0,1,2,\ldots \quad (2)$$

hence

$$L = \frac{hr}{\lambda} = \frac{nh}{2\pi} \text{ and } L = n\hbar \quad (3)$$

therefore

$$E = \frac{n^2 h^2}{2I} \text{ with } n = 0,1,2,\ldots \quad (4)$$

Real molecules

The rotation of a body in 3-D can be broken down in three components, being their directions relative to the three normal axes, with the origin at the centre of gravity. Therefore, it has three principal inertia moments, one for each axis: I_a, I_b and I_c.

We can classify the molecules in three different groups according to the relative values of the three inertia moments. Each group has a characteristic rotation spectra.

Linear, diatomic and polyatomic molecules, asymmetric molecules and spherical top molecules.

Linear Molecules

All atoms are located in a straight line. Hence $I_b=I_c$; $I_a=0$ (approximation for I_a).

Rigid Rotor Approximation (Rigid diatomic molecule)

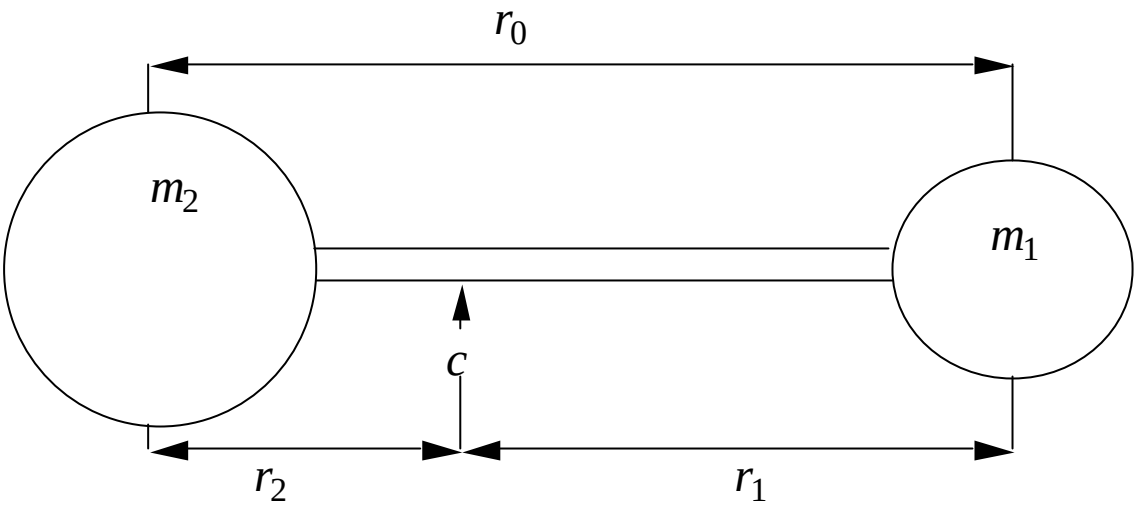

Fig 3. The molecule rotates around c, where c is the centre of gravity, and $r_0=r_1+r_2$. The centre of gravity and the moment of inertia, I, are defined by:

$$m_1r_1=m_2r_2 \quad \text{and} \quad I=\sum m_i r_i^2 \quad (5)$$

then $I=\mu r_0^2$, where μ is called the reduced mass of the system, given by:

$$\mu = \frac{m_1 m_2}{m_1 + m_2} \quad (6)$$

Using the Schrodinger equation, $\left(-\frac{\hbar^2}{2mr^2}\right)\Lambda^2\Psi = E\psi$ we obtain:

$$E=\left(\frac{\hbar^2}{2I}\right)J(J+1) \quad (7)$$

Λ^2 is the Legendrian using spherical co-ordinates.

Then

$$E=\frac{h^2}{8\pi^2 I}J(J+1) \text{ Joules, where } J=0,1,2,\ldots \quad (8)$$

h = Planck constant and $I = I_C$ or I_C and J is the rotational quantum number.

Since $\nu = \frac{\Delta E}{h}$ Hz and $\bar{\nu} = \frac{\Delta E}{h}$ cm^{-1} then

$$\bar{E}_J = \frac{E_J}{hc} = \frac{h}{8\pi^2 Ic}J(J+1) \quad J=0,1,2,\ldots \quad (9)$$

c is the velocity of light.

Therefore

$$\bar{E}_J = \bar{B}J(J+1)\ cm^{-1},\ J = 0,1,2,\ldots , \qquad (10)$$

where $\bar{B}$ is the rotational constant and has the value:

$$\bar{B} = \frac{h}{8\pi^2 Ic}\ cm^{-1} \qquad (11)$$

$I = I_B$ or I_C and c is in cm s^{-1}

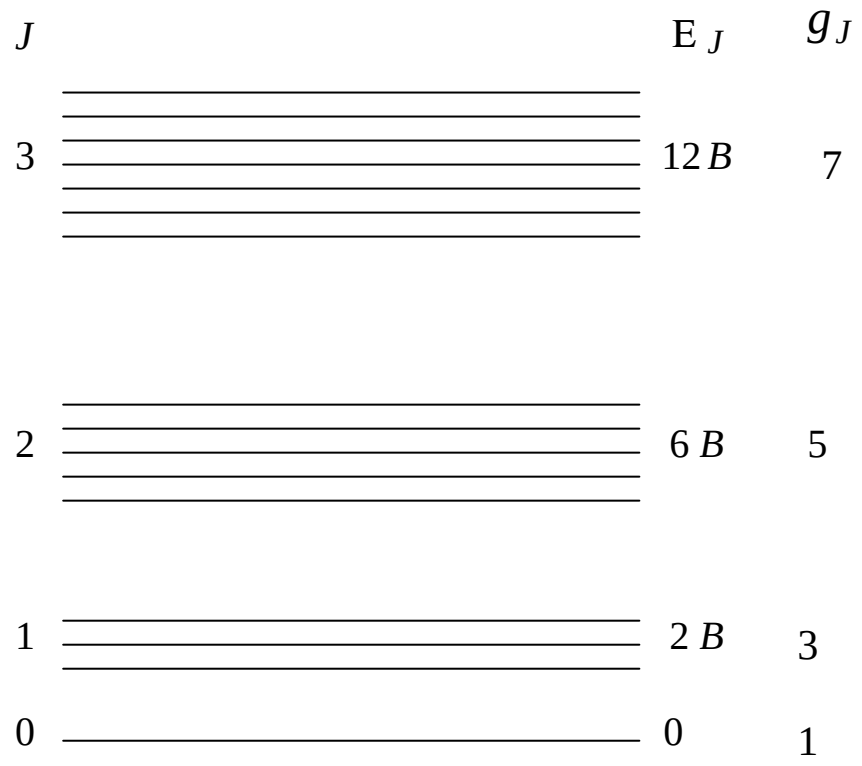

Fig 4. The allowed rotational energies of a rigid diatomic molecule, showing the (2J+1) degeneracy.

The selection rule for transitions by a photon is $\Delta J = \pm 1$. For the promotion from state J to state J+1 we have

$$\omega_J = E_{J+1\leftarrow J} = E_{J+1} - E_J = 2B(J+1)\ cm^{-1} \qquad (12)$$

Then, the transitions between the energy levels of a rigid diatomic molecule and the spectrum which arises from them have the shape, fig 5:

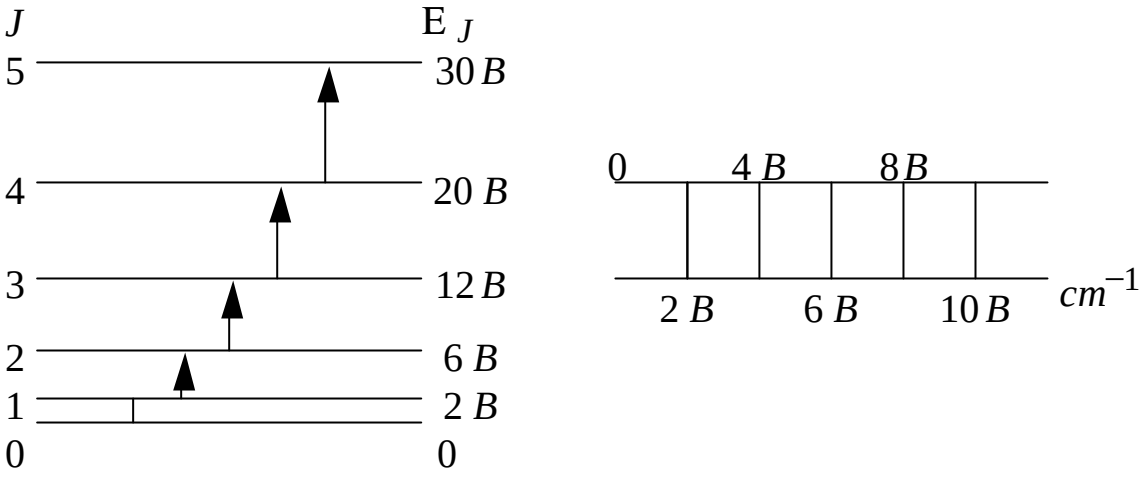

The transition intensity is proportional to the square of the transition moment which is given by:

$$R_r = \int \Psi_r^{n*} \mu \Psi_r^{m} d\tau \qquad (13)$$

The rotational selection rules the conditions for which the intensity, and therefore R_r, is non-zero.

This selection rules are:
1.- The molecule must be have a permanent dipole moment $\mu \neq 0$
2.- $\Delta J = \pm 1$
3.- $\Delta M_J = 0, \pm 1$, a rule which is important only if the molecule is in an electric or magnetic field.

1.- Only if the molecule is asymmetric (heteronuclear) will the spectrum be observed, since if it is homonuclear there will no dipole component change during the rotation, and hence no interaction with radiation.

2.- A more sophisticated application of Schrodinger equation shows that, for this molecule, we need only consider transitions in which J changes by one unit, all other transitions being spectroscopically forbidden.

3.- Setting out from $E_J = \frac{h}{8\pi^2 I} J(J+1)$ Joules, the angular momentum is given by:

$$P_J = [J(J+1)]^{1/2} \hbar \qquad (14)$$

In general, J is associated with the total angular momentum, i.e. rotational plus orbital plus electron spin, but when there is no orbital or electron spin angular momentum, it refers simply to rotation.
Just as with other angular moment there is space quantization of rotational angular momentum so that the Z component is given by

$$(P_J)_z = M_J\hbar \qquad M_J = J, J-1, \ldots, -J \qquad (15)$$

Therefore, in the absence of an electric or magnetic field, each rotational energy level is $(2J+1)$-fold degenerate.

The intensities of spectral lines

A first factor governing the population of the levels is the Boltzmann distribution term in energy given by:

$$\exp(-E_J / kT) = \exp[-BJ(J+1)/kT] \qquad (16)$$

A second factor is the possibility of degeneracy in the energy states. Degeneracy is the existence of two or more energy states which have exactly the same energy. In the case of the diatomic rotator we may approach the problem in terms of its angular momentum.

$$E = \frac{1}{2}I\omega^2 \qquad (17)$$

$$P = I\omega \qquad (18)$$

where ω is the rotational frequency (rad s^{-1}).

Then

$$P = \sqrt{2EI} \quad \text{and} \quad 2EI = J(J+1)\frac{h^2}{4\pi^2} \qquad (19)$$

and hence

$$P = [J(J+1)]^2\hbar \quad J = 0,1,2,\ldots \qquad (20)$$

Since each energy level is $(2J+1)$-fold degenerate. Then the population N_n of the nth level relative to N_0 is obtained from Boltzmann's distribution law, and gives:

$$\frac{N_J}{N_0} = (2J+1)\exp\left(-\frac{E_J}{kT}\right) = (2J+1)\exp\left(-\frac{BJ(J+1)}{kT}\right) \qquad (21)$$

Differentiation of this equation shows that the population is a maximum at the nearest integral J value to:

$$\text{Maximum population} = J_{max} = \left(\frac{kT}{2hB}\right)^{1/2} - \frac{1}{2} \qquad (22)$$

Centrifugal distortion

An important effect when the molecules rotate is centrifugal distortion. The atoms are subject to centrifugal forces that distort the molecular geometry and therefore change the moments of inertia. In the case of a diatomic molecule, the centrifugal distortion stretches the bond, and therefore increases the moment of inertia; as a result, the energy levels are less far apart than predicted by:

$$E_J = BJ(J+1) \qquad (23)$$

The Schrodinger wave equation may be set up for a non-rigid molecule, and the rotational levels are found

$$E_J = \frac{h^2}{8\pi^2 I} J(J+1) - \frac{h^4}{32\pi^4 I^2 r^2 k} J^2(J+1)^2 \text{ Joules} \qquad (24)$$

or

$$E_J = \frac{E_J}{hc} = BJ(J+1) - DJ^2(J+1)^2 \text{ cm}^{-1} \qquad (25)$$

and D is defined as centrifugal distortion constant given by

$$D = \frac{h^3}{32\pi^4 I^2 r^2 kc} \text{ cm}^{-1} \qquad (26)$$

which is a positive quantity, and k is the force constant for simple harmonic motion:

$$k = 4\pi^2 \bar{\omega}^2 c^2 \mu \qquad (27)$$

where $\bar{\omega}$ is the vibration frequency in cm^{-1}.

From

$$\bar{B} = \frac{h}{8\pi^2 c\mu r^2} \quad \text{and} \quad \bar{D} = \frac{h^3}{32\pi^4 I^2 r^2 kc}$$

we obtain

$$\bar{D} = \frac{16 B^3 \pi^2 \mu c^2}{k} = \frac{4B^3}{\bar{\omega}^2} \qquad (28)$$

Then, the centrifugal distortion (for a diatomic molecule) constant is related to the vibrational wavenumber of the bond (which is a measure of its stiffness) and so the observation of the convergence of the rotational levels as J increases can be interpreted in terms of the rigidity of the bond.

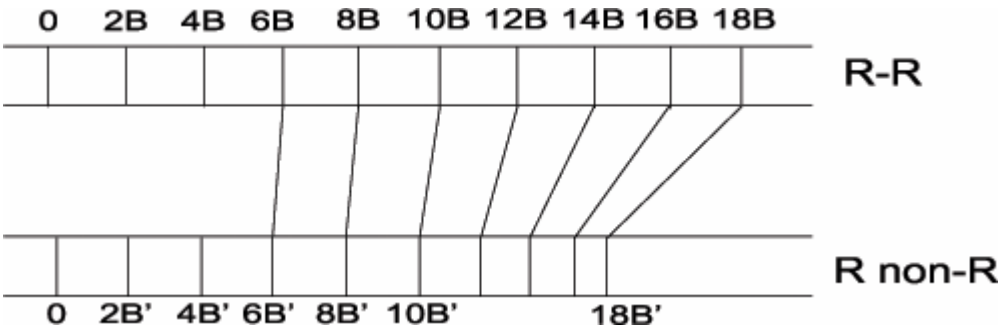

Fig 6. The change in the rotational energy levels and spectrum when passing from a rigid to a non-rigid diatomic molecule.

This spectrum comes from, fig 7:

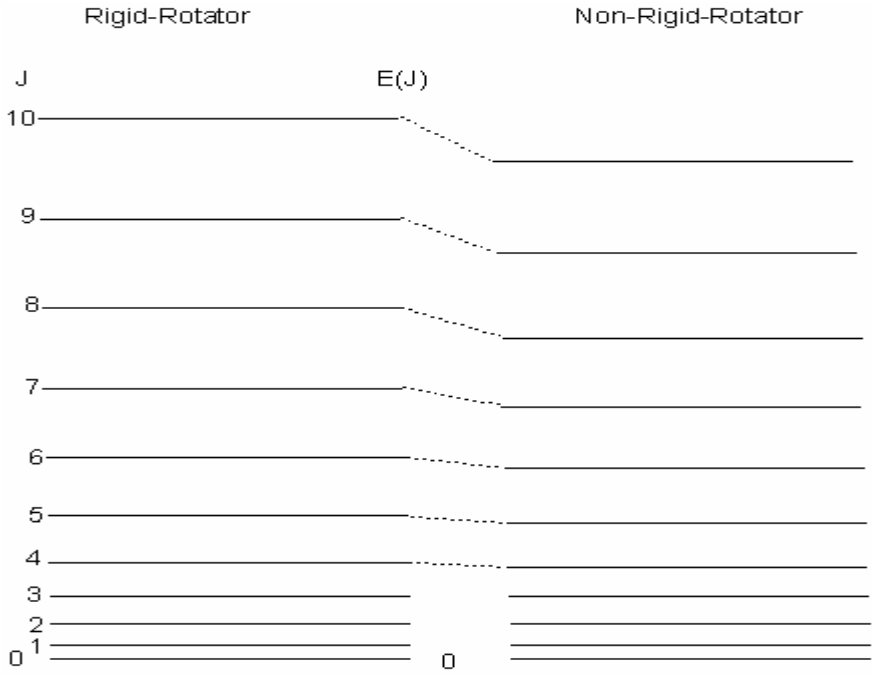

Vibration motion

For the study of vibrational we consider where compression and extension of the bond may be likened to the behaviour of a spring, obeying Hooke's Law. Then, we may write:

$$F = -k(r-r_{eq}) \quad (29)$$

where k is the force constant, F is the restoring force, r the internuclear distance and r_{eq} where the internuclear distance is a minimum of energy of the bond. In this case, the energy curve is a parabolic and has the form:

$$E = \frac{1}{2}k(r-r_{eq})^2 \qquad (30)$$

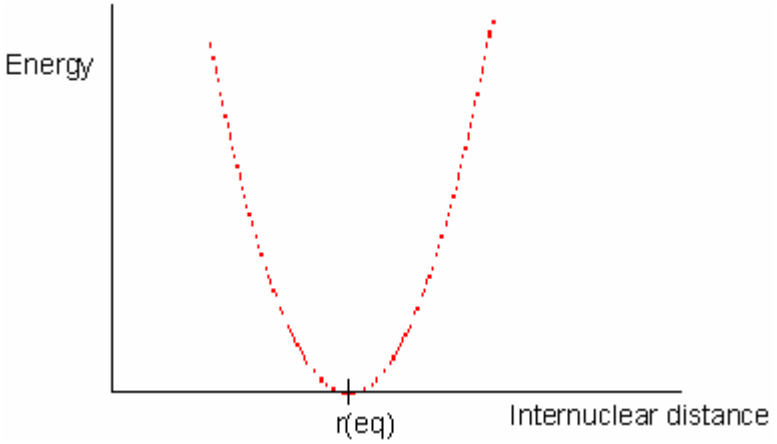

Fig 8.

This model of vibrating diatomic molecule is called simple harmonic oscillator model. If the energy of the molecule increases, the oscillation will be more vigorous, i.e. the degree of compression and extension will be greater, but the vibrational frequency will not change. A bond, like a spring, has an intrinsic vibrational frequency, dependent of the mass of the system and the force constant, but is independent of the amount of distortion. Classically:

$$\bar{\omega} = \frac{1}{2\pi c}\sqrt{\frac{k}{\mu}} \quad cm^{-1} \qquad (31)$$

Vibrational energies are quantized, and using the Schrodinger equation:

$$-\frac{\hbar^2}{2m}\times\frac{d^2\Psi}{dx^2}+\frac{1}{2}kx^2 = E\Psi$$

we may calculate them for any particular system:

$$E_\upsilon = \left(\upsilon+\frac{1}{2}\right)\hbar\omega \quad \text{Joules } \upsilon = 0,1,2,\ldots \qquad (32)$$

ω is the angular frequency, υ is the quantum number for the vibrational motion.

$$\varepsilon_\upsilon = \frac{E_\upsilon}{hc} = \left(\upsilon+\frac{1}{2}\right)\bar{\omega} \quad cm^{-1} \quad \upsilon = 0,1,2,\ldots \qquad (33)$$

$\bar{\omega} = \frac{\omega}{c}$ giving the energies allowed for a simple harmonic vibrator

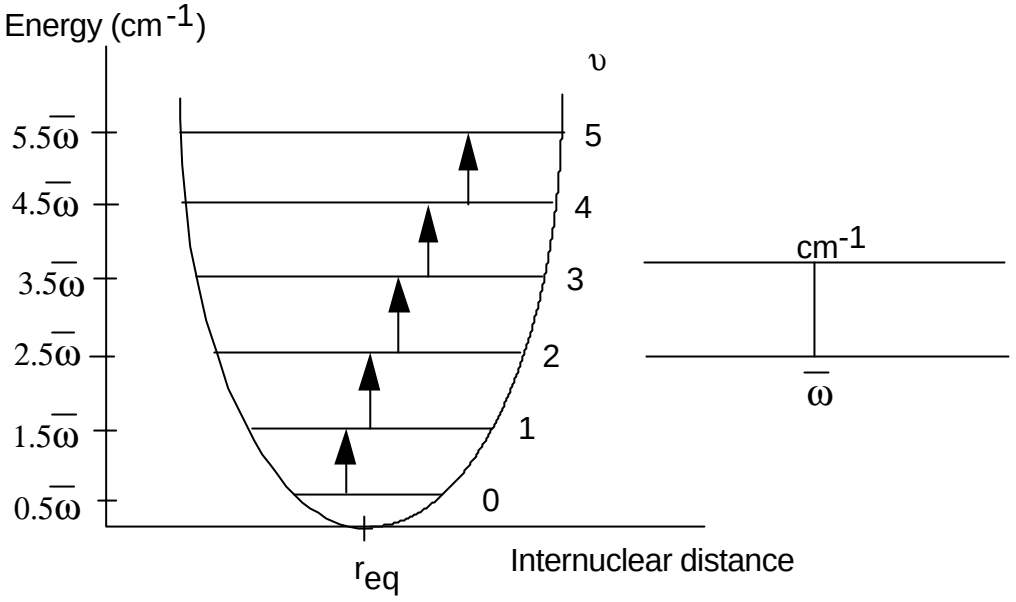

Fig 9. The vibrational energy levels and allowed transitions between them for a diatomic molecule undergoing simple harmonic motion.
As we can see, the zero-point energy does not corresponds with zero vibrational energy: $0.5\overline{\omega}$ in cm^{-1} for $\upsilon = 0$, which is the minimum vibrational quantum number, and depends only on the classical vibration frequency, and hence on the strength of the chemical bond and the atomic masses.
Further use of the Schrodinger equation leads to the selection rule for the harmonic oscillator undergoing vibrational changes:

$$\Delta\upsilon = \pm 1 \quad (34)$$

Moreover, we must bear in mind that the observable spectrum is produced with the condition of that the molecule must be heteronuclear diatomic since the vibration involves a change in the dipole moment and homonuclear molecules do not have one.

Applying the selection rule, we have:

$$\Delta\varepsilon = \varepsilon_{\upsilon+1\leftarrow\upsilon} = \varepsilon_{\upsilon+1} - \varepsilon_{\upsilon} = \hbar\overline{\omega} \quad cm^{-1} \qquad (35)$$

for absorption and

$$\Delta\varepsilon = \varepsilon_{\upsilon+1\rightarrow\upsilon} = \varepsilon_{\upsilon+1} - \varepsilon_{\upsilon} = \hbar\overline{\omega} \quad cm^{-1} \qquad (36)$$

for emission. Therefore, the vibrational levels are equally spaced and hence the transitions between any two neighbouring states will have the same energy change, and we can obtain the wavenumber of the spectral line absorbed or emitted through of that difference between energy levels expressed in cm^{-1}.

$$\bar{\nu}_{spectroscopic} = \varepsilon = \bar{\omega} \ \ cm^{-1} \qquad (37)$$

The explanation is that in absorption, for instance, the vibrating molecule will absorb energy only from radiation with which it can interact and this must be radiation of its own oscillation frequency.

But real molecules do not obey exactly the laws of simple harmonic motion. If the bond between atoms is stretched, for example, there will be a point at which it will break. an empirical expression, which fits this curve to a good approximation, is the Morse function:

$$E = D_{eq}\left[1 - \mathbf{exp}\left\{a\left(r_{eq} - r\right)\right\}\right]^2 \qquad (38)$$

Where "a" is a constant for a particular molecule and D_{eq} is the dissociation energy.

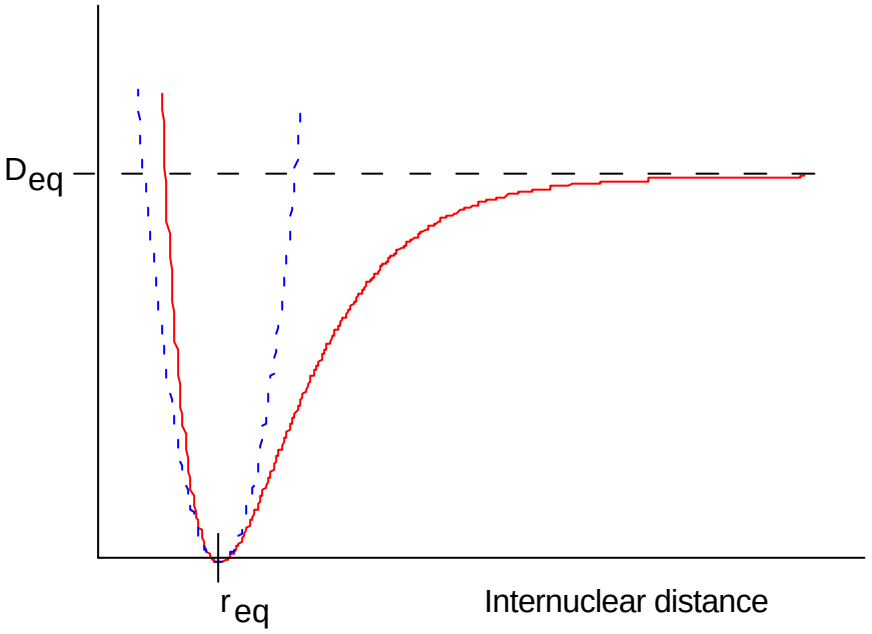

Fig 10. The Morse curve: the energy of a diatomic molecule undergoing anharmonic extensions and compressions.
The dashed curve is the ideal simple harmonic vibration parabola.

Using the Morse equation in the Schrodinger equation, the pattern of allowed vibrational energy levels is given by:

$$\varepsilon_\upsilon = \left(\upsilon + \frac{1}{2}\right)\overline{\omega}_e - \left(\upsilon + \frac{1}{2}\right)^2 \overline{\omega}_e x_e \quad \text{cm}^{-1} \quad \upsilon = 0,1,2,\ldots \quad (39)$$

Where x_e is the corresponding anharmonicity constant, which, for bond stretching vibrations is always small and positive ($\approx +0.01$), so that the vibrational levels crowd more closely together with increasing υ.
Note that this equation is only an approximation, because more precise expressions require cubic, quartic, etc., ... terms in $\left(\upsilon + \frac{1}{2}\right)$ with anharmonic constants y_e, z_e, etc., but this terms are important only at large values of υ.

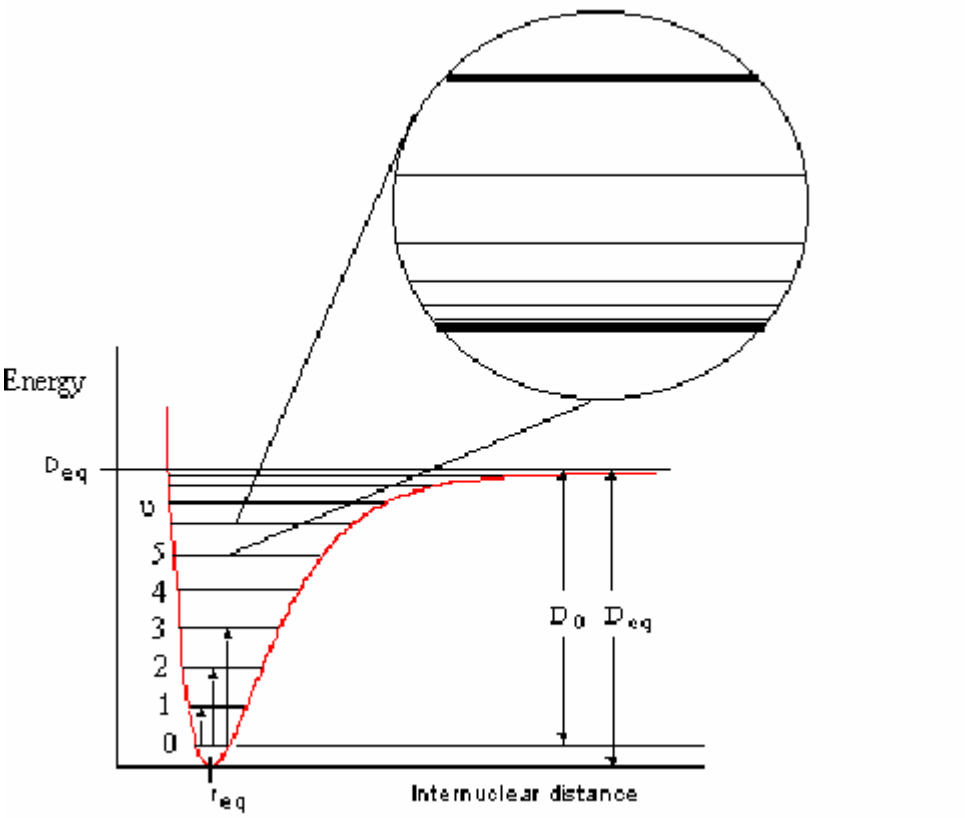

Fig 11. The picture shows vibrational levels and rotational fine structure superimposed on the Morse potential. D_0 is the dissociation energy from the ground vibrational level.

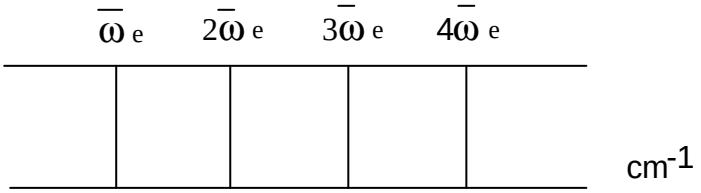

Fig 12. The vibrational energy levels and some transitions between them for a diatomic molecule undergoing anharmonic oscillations.

To define $\overline{\omega}_e$, oscillation frequency, we rewrite the equation for ε_υ for the anharmonic oscillator, as

$$\varepsilon_\upsilon = \overline{\omega}\left\{1 - x_e\left(\upsilon + \frac{1}{2}\right)\right\}\left(\upsilon + \frac{1}{2}\right) \quad (40)$$

and we compare it with the energy levels of the harmonic oscillator, then:

$$\overline{\omega}_a = \overline{\omega}_e\left\{1 - x_e\left(\upsilon + \frac{1}{2}\right)\right\} \quad (41)$$

$\overline{\omega}_a$ is the oscillation frequency for the anharmonicity and is smaller than that for the harmonic case.
We can see that the anharmonic oscillator behaves like the harmonic oscillator but with an oscillation frequency, which decreases steadily with increasing υ. If we replace υ by

$$\upsilon = -\frac{1}{2} \quad (42)$$

(an hypothetical state), then $\varepsilon = 0$, so the molecule would be at the equilibrium point with zero vibrational energy. Its oscillation frequency (in cm^{-1}) would be:

$$\overline{\omega}_a = \overline{\omega}_e \quad (43)$$

Then, $\overline{\omega}_e$ may be defined as the (hypothetical) equilibrium oscillation frequency of the anharmonic system, i.e., the frequency for infinitely small vibrations about the equilibrium point.
For any real state specified by a positive integral υ, the oscillation frequency will be given by (1), then for υ =0 we have:

$$\overline{\omega}_0 = \overline{\omega}_e\left(1 - \frac{1}{2}x_e\right) \ cm^{-1} \quad (44)$$

and

$$\varepsilon_0 = \frac{1}{2}\overline{\omega}_e\left(1 - \frac{1}{2}x_e\right) \ cm^{-1} \quad (45)$$

therefore the zero-point energy differs slightly from that for the harmonic oscillator.
The selection rules for the anharmonic oscillator are found to be:

$$\Delta\upsilon = \pm 1, \pm 2, \pm 3, \ldots \quad (46)$$

but only the lines $\Delta\upsilon = \pm 1, \pm 2$ and ± 3 have observable intensity, and this is predicted by theory and observed in practice.

An important consideration is that a diatomic molecule can execute rotations and vibrations, independently of the electronic state, using the Born-Oppenheimer approximation. Then, we assume that the combined rotational-vibrational energy is simply the sum of the separate energies:

$$\varepsilon_{total} = \varepsilon_{rot} + \varepsilon_{vib} \qquad (47)$$

Then, taking the separate expressions for ε_{rot} and ε_{vib}, we have:

$$\varepsilon_{J,\upsilon} = \varepsilon_J + \varepsilon_\upsilon \qquad (48)$$

So:

$$\varepsilon_{J,\upsilon} = BJ(J+1) - DJ^2(J+1)^2 + \left(\upsilon + \frac{1}{2}\right)\overline{\omega}_e - x_e\left(\upsilon + \frac{1}{2}\right)^2 \overline{\omega}_e \quad \text{in cm}^{-1}. \qquad (49)$$

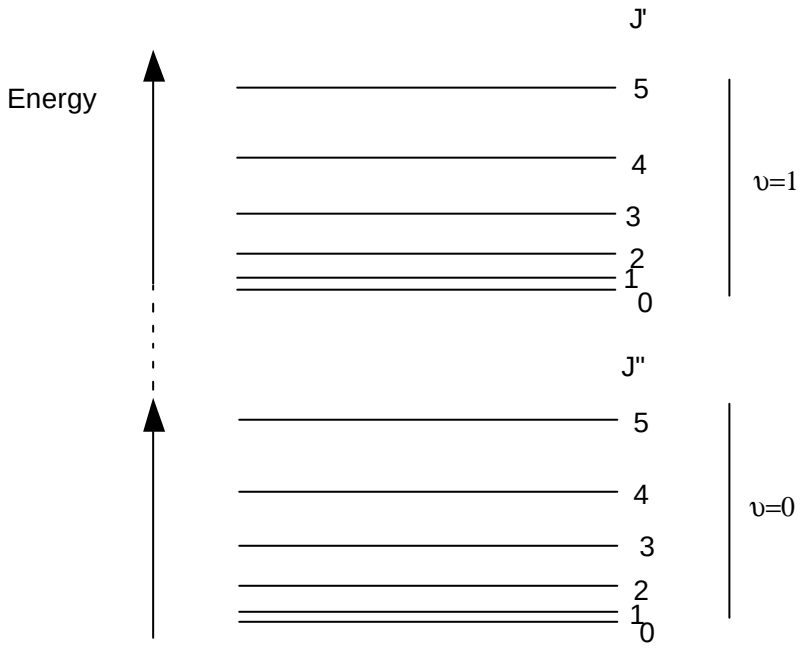

Fig 13. The electronics levels are more widely spaced than vibrational and rotational levels. They are bands, consisting of a series of vibrational (and rotational) transitions within the electronic transition. A series of vibrational transitions from one initial vibrational state (in the lower electronic state) to a number of different final vibrational states (within the final electronic state) is called a Franck-Condon progression, and the intensity distribution within this progression is determined by the difference in equilibrium bond length of the molecule in the two electronic states.

Franck-Condon Principle

Since the nuclei are so much more massive than the electrons, an electronic transition takes place faster than the nuclei can respond. Then, after the transition, electron density is rapidly built up in new regions of the molecule, and the stationary nuclei, suddenly, experience a new force field. Then the nuclei start to oscillate from their original separation, therefore, the stationary equilibrium separation of the nuclei in the initial electronic state becomes the turning point, which corresponds to the point of a vibration where the nuclei are classically stationary, in the final electronic state.
Quantum Mechanically, this allows us to calculate the intensities of the transitions to different vibrational levels of the electronically excited molecule and, then, to account for the shape of the absorption band.

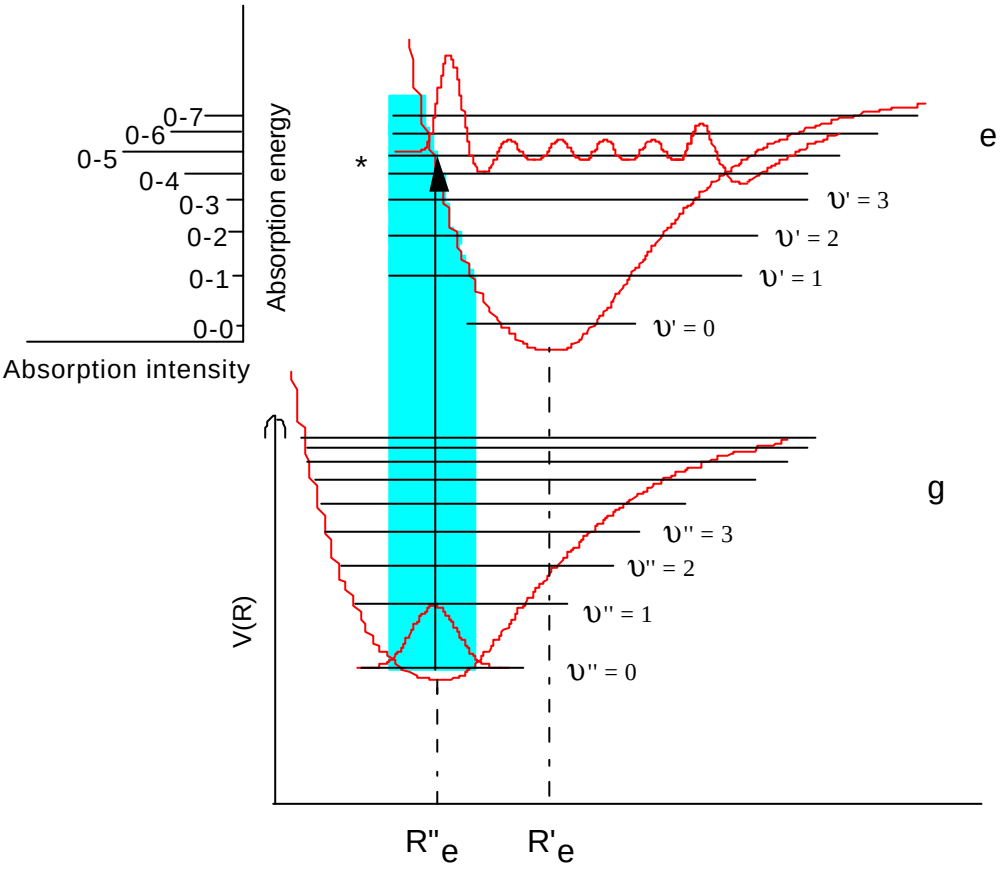

Fig 14. The form of the vibrational wavefunction shows that the most probable location of the nuclei is at their equilibrium separation, R_e for V=0.

The electronic transition, hence, is most likely to take place when the nuclei have this separation. The nuclear framework remains constant during this excitation, and the

electronic transition occurs without change of nuclear geometry along the vertical transition. The level marked with * is the one in which the nuclei are most probably at the initial separation, R_e, because the vibrational wavefunction has the maximum amplitude there, and so this is the most probable level for the termination of the transition.

The Franck-Condon Principle for absorption

"The electron jump in a molecule takes place so rapidly in comparison to the vibrational motion that immediately afterwards the nuclei still have very nearly the same relative position and velocity as before the jump".

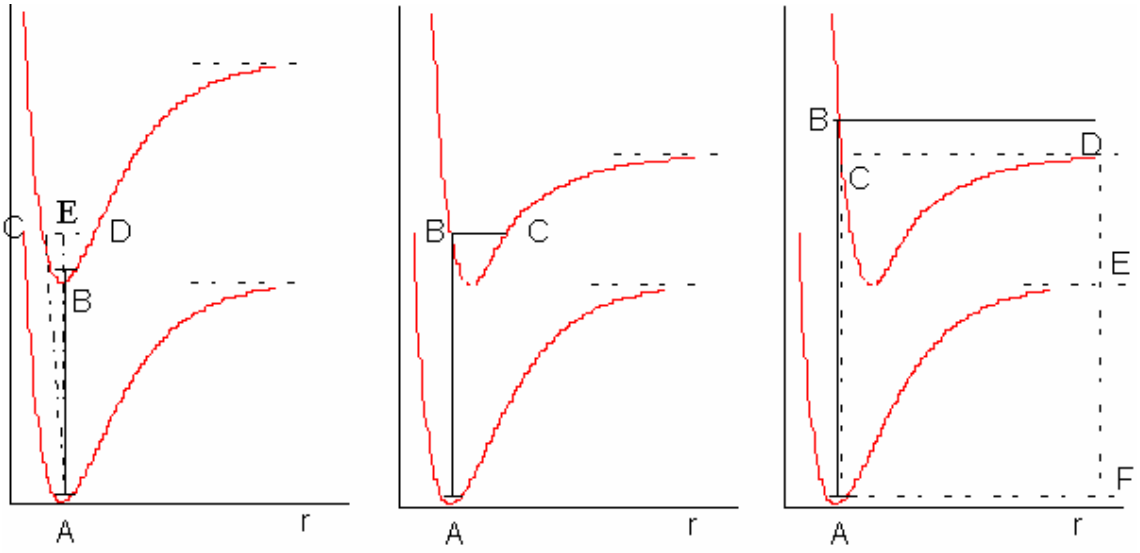

a) b) c)

Fig 15. Potential curves explaining the intensity distribution in absorption according to the Franck-Condon principle. In c), AC gives the energy of the dissociation limit, EF the dissociation energy of the ground state, and DE the excitation energy of the dissociation products.

The potential curves of the two electronic states (in a)) have been so chosen that their minima lie very nearly one above the other (equal internuclear distance). In absorption, the molecule is initially at the minimum of the lower potential curve, if we disregard the zero point vibration. Due to the Franck-Condon principle a transition between the lowest levels in the ground and upper state will have only small changes in position and momentum. However, a transition into a high vibrational state, CD, would be possible only when, at the moment of the electronic jump, either the position (transition from A to C) or the velocity (transition from A to E) or both alter to an appreciable extent. At the point E the molecule has the amount of kinetic EB. Only at the turning point C or D are the velocity and the kinetic energy zero, as the initial state at A. Hence, following the Franck-Condon principle a transition from $v''=0$ to such a high vibrational level is forbidden or at least highly improbable. For the level $v'=1$, the necessary alteration of the position or the velocity during the electron jump is comparatively small.

In b), the minimum of the upper potential curve lies at a somewhat greater r value than of the lower. Therefore the transition between the minima of the two electronic states is no longer the most probable, since the internuclear distance must alter somewhat in such a transition. The most probable transition is from A to B. For this transition there is no change in the internuclear distance at the moment of the jump and no change of the velocity. Hence, after the transition, the two nuclei still have their old distance from each other and the same relative velocity. But now, the equilibrium internuclear distance has a different value in the new electronic state, the nuclei start to vibrate between B and C. The vibrational levels whose left turning points lie in the neighbourhood of B are the upper levels of the most intense bands. For still higher vibrational levels an appreciable change of the internuclear distance or velocity must take place, as a result of which the intensity of the bands decrease again with increasing v'.

In c) the minimum of the upper potential curve lies at a still greater internuclear distance. The Franck-Condon principle is strictly fulfilled for the transition AB. However, the point B on the upper potential curve lies above the asymptote of this curve and therefore corresponds to the continuous region of the vibrational spectrum of the upper state.

Therefore, it can be said that in absorption the most intense transition from $v''=0$ is always that corresponding to a transition from the minimum of the lower potential curve vertically upward.

The Franck-Condon Principle for Emission

According to the Franck-Condon principle, the variation of intensity in a band progression with $v'=0$ in emission corresponds exactly to that of a progression with $v''=0$ in absorption. But, actually, there are some differences: There is an intensity maximum at v'' value that is determined by the relative position of the minima of the two potential curves and their shape.
However, the intensity distribution is different for band progressions in emission having v' different to zero.

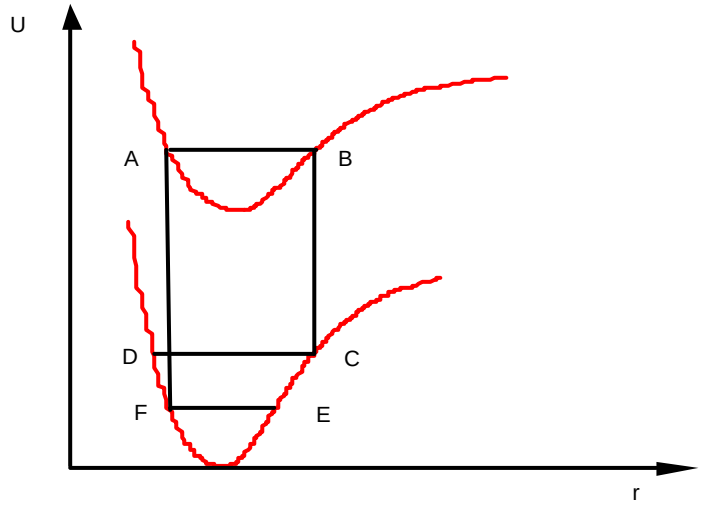

Fig 16. During the vibration in the upper state the molecule is on line AB and when it emits, if the molecule is at B, and if there is to be no change in position and velocity, immediately after the jump the molecule take place over C, at the turning point for the new vibrational motion CD, but the electron can jump from A to F, and form the left turning point of the new vibrational motion EF. Therefore, we can see that there are two v'' values for which the probability of the transition from a given v' is a maximum; that is, there are two intensity maxima to be expected in a v''-progression, one at small v'' and a second at large v''.

The quantitative basis of the Frank-Condon principle is the transition dipole moment integral. In order to deal with the vibronic transitions, we have to consider the total electronic and vibrational wavefunctions of the initial and final states. In terms of the Born-Oppenheimer approximation, these can be approximated as a product of electronic and vibrational wavefunctions. Then, for an electronic state, ε, and vibrational state, ν, the transition dipole moment for the excitation $\varepsilon', \nu' \leftarrow \varepsilon, \nu$ is therefore approximately:

$$\mu = -e\int \{\Psi_{\varepsilon'}(r)\Psi_{\nu'}(R)\}^* r\{\Psi_{\varepsilon}(r)\Psi_{\nu}(R)\}d\tau_{elec}\,d\tau_{nuc} \qquad (50)$$

$$= -e\int \Psi^*_{\varepsilon'}(r) r \Psi_{\varepsilon}(r) d\tau_{elec} \int \Psi^*_{\nu'}(R)\Psi_{\nu}(R) d\tau_{nuc} \qquad (51)$$

Where r stands for the electronic coordinates and R for the nuclear coordinates.
The second integral is the overlap integral, $S_{\nu',\nu}$ between the initial and final vibrational state wavefunctions. Since the intensity of a transition depends on the square of the transition dipole moment, the vibronic transition intensity depends on $S^2_{\nu',\nu}$, which is known as the Franck-Condon factor for the $\varepsilon', \nu' \leftarrow \varepsilon, \nu$ transition: $\int \Psi^*_{\nu}\Psi_{\nu} d\tau$

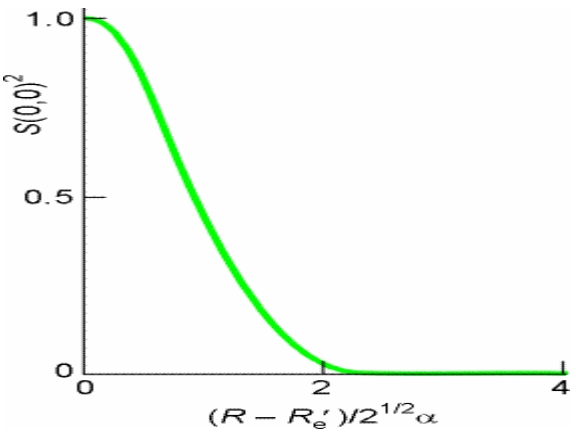

Fig 17. The variation of the Franck-Condon factor as the difference between the bond lengths of the lower and upper vibrational states increases.

Fundamentals of Fluorescence

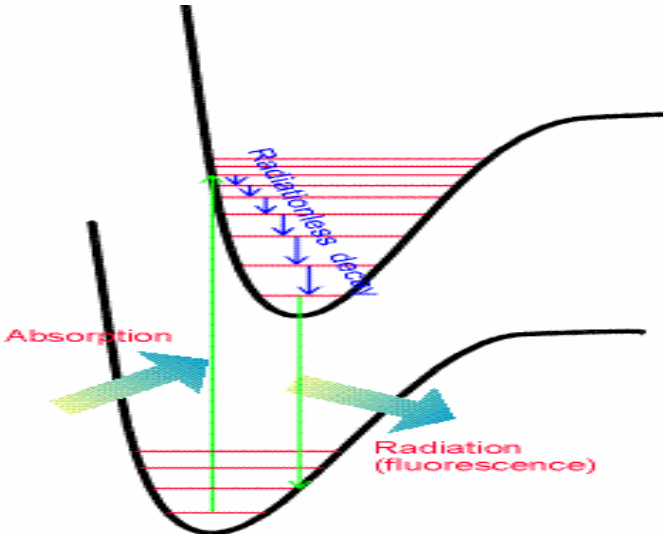

Fig 18. The initial absorption takes the molecule to an excited electronic sate. In this state, the molecule is subjected to collisions with the desorbed molecules from the surface and this produce a ladder down to a lower vibrational level. The surrounding molecules may be unable to remove the large energy needed to relax the molecule to the ground electronic state, and it may survive long enough to undergo spontaneous emission, emitting the remaining excess energy as radiation. The downward electronic transition is vertical (in accord with Frank-Condon principle) and the fluorescence spectrum possesses a vibrational structure characteristic of the lower electronic state. The fluorescence occurs at a lower frequency than the incident light: the radiation occurs after some vibrational energy has been discarded into the surroundings.

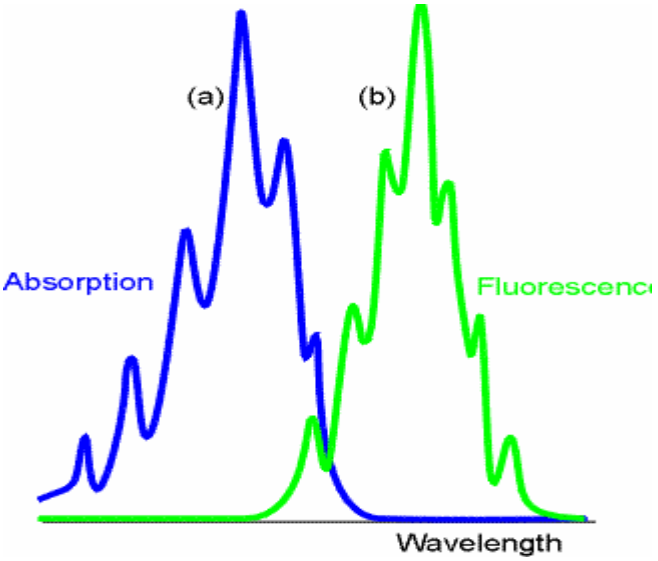

Fig 19

a) The absorption spectrum shows a vibrational structure characteristic of the upper state.
b) The fluorescence spectrum shows a structure characteristic of the lower state; it is also displaced to lower frequencies (but the 0-0 transitions are coincident) and resembles a mirror image of the absorption.

Introduction to laser action

Laser action, as the acronym light amplification by stimulated emission of radiation suggests, depends on emission by a stimulated process.

Laser action is schematically, fig 20

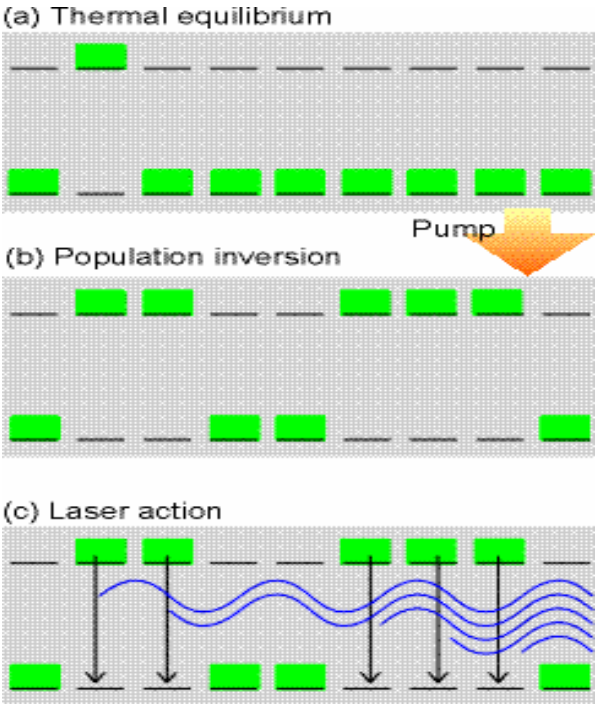

a) Equilibrium population: The Boltzmann population of states, with more atoms in the ground state.
b) Inverted population: When the initial states absorbs, the populations are inverted (the atoms are pumped to the excited state)
c) Laser action: A cascade of radiation then occurs, as one emitted photon stimulates another atom to emit, and so on. The radiation is coherent (phases in step).

By some means a majority of molecules are excited (pumped) into an upper state. The sample is contained in a cavity between two mirrors, and when a molecule emits spontaneously the photon it generates is reflected backwards and forwards between them. Its presence stimulates other molecules to emit, and they add more photons of the same frequency to the cavity, and these stimulate more molecules to emit then the cascade of energy builds up rapidly.

The characteristics of laser light reflect how it is generated: it is monochromatic (because photons stimulate emission of more photons of the same frequency), coherent

(because the phases of the electric fields of the radiation are in step), and non-divergent (because photons travelling at an angle to the cavity axis are not trapped and do not stimulate others).

Apparatus [6,7]

The experimental apparatus used for the etching of GaAs with halogens is designed to deposit a short pulsed of halogen onto a GaAs surface and then detect the products desorbed from the surface using a mass spectrometer, as a function of time.

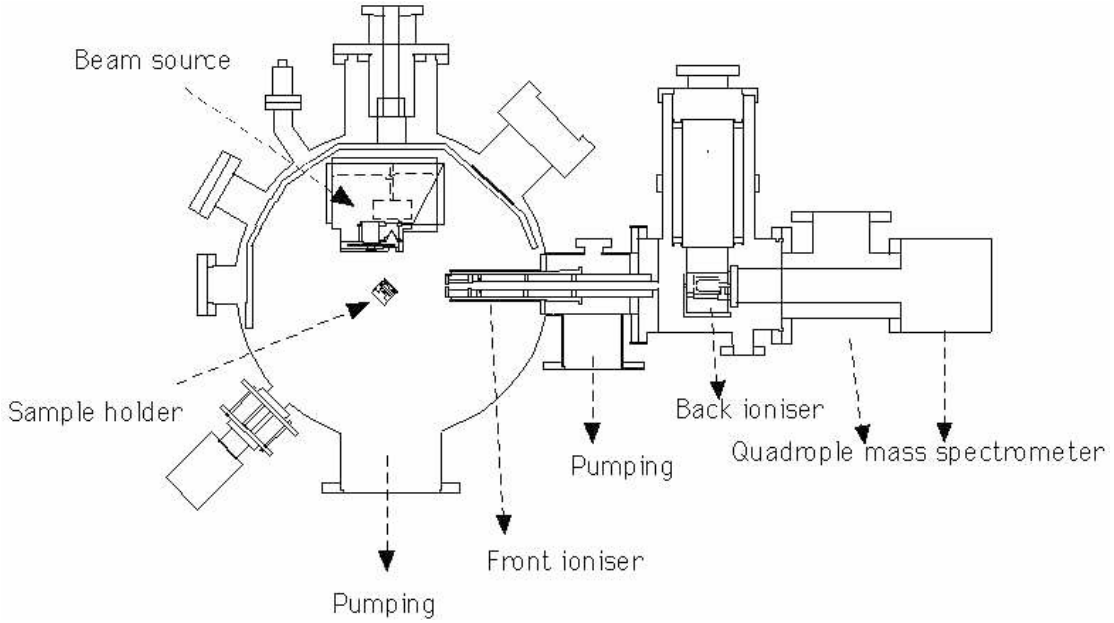

Fig 1. The apparatus provides different beam incident and product desorption angles.

The main chamber houses the GaAs sample, where the reaction between the sample and the molecular beam takes place; it also contains the RHEED apparatus and the front ioniser of the detector. The chamber also has a liquid nitrogen cryotrap and to a diffusion pump to achieve the necessary vacuum. The pump is isolated from the main chamber by a quarter swing butterfly valve.
Below the chamber and used to achieve the high vacuum are the diffusion pumps, and a rotatory pump for the gas handling apparatus. The ultimate pressure required is about 10^{-7}-10^{-8} torr or lower. For surface reactions, the requirement is to prevent contamination of the surface, so the vacuum has to be much lower, preferably 10^{-10} torr. The diffusion pump achieves a pressure around 10^{-9} torr, then a large surface area liquid nitrogen filled cryotrap is used to obtain the optimum vacuum. In the diffusion pump a heater vaporises the working fluid, which arises inside the vapour chimney and is deflected downwards by the jet assembly in an annular jet at supersonic speed. This high-speed jet of fluid of molecules imparts a momentum to the random moving incoming gas molecules giving them a direction primarily towards the region of the pump outlet where they are removed by a mechanical pump. The vapour jet condenses on the cooled pump walls and returns to the boiler. This pump operates in the molecular flow region. Diffusion pumps suffer from two defects whereby the pump fluid enters the vacuum enclosure: the back-streaming, and the back-migration. The first is due to a

small fraction of molecules of the working oil moving from the top jet in the wrong direction (toward the chamber). The second is due to re-evaporation of the working oil from the walls of the pump and the connecting tube to the chamber.

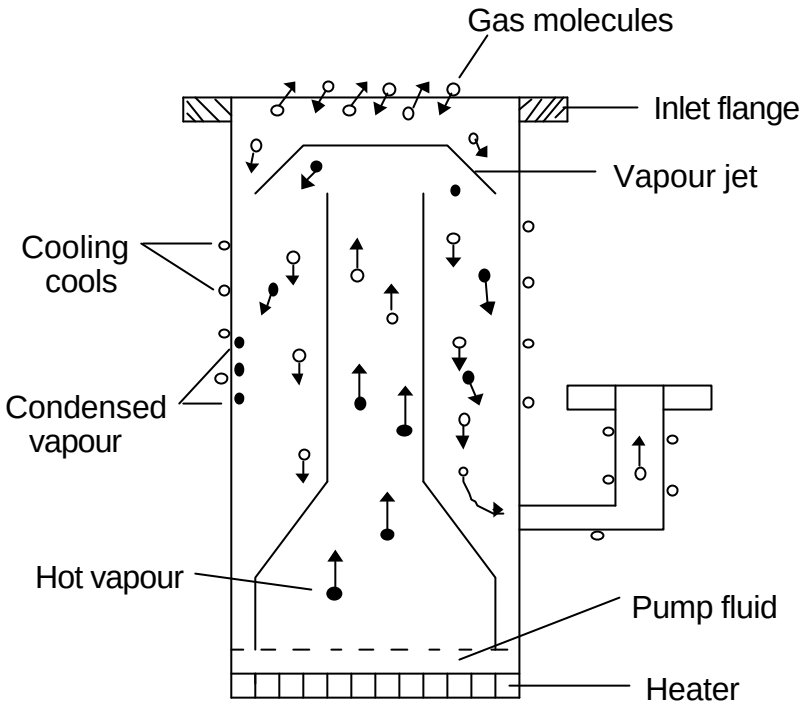

Fig 2 Schematic diagram of a cross-section of a difussion pump

A second pump, in this case a rotatory pump, is connected to the diffusion pump with the functions to maintain the required backing pressure for correct operation of the diffusion pump, and to enable the chamber to be pumped out from atmospheric pressure to the starting pressure of the diffusion pump. To start the system, the isolation and roughing valves are closed and the backing valve is opened. The rotatory pump is started and evacuates the diffusion pump body to less than 10 mbar when its heaters can be switched on.

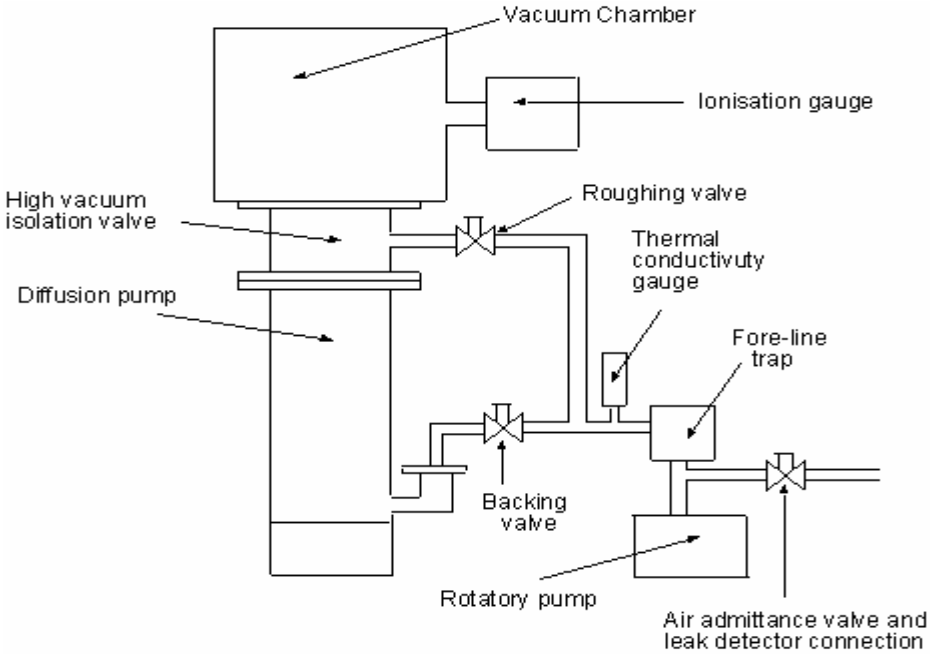

Fig 3. Typical diffusion pump system

The pulsed beam source is mounted in the source chamber, which is behind the main chamber. A rotating plate separates both chambers. The pulse beam assembly and plate can rotate freely, allowing the beam to hit the surface at a range of angles. When the beam and sample are locked at a particular angle, it is the beam source that is rotated to measure the angular distribution of the products. An absolute angle optical encoder is used to measure the angle of the pulse beam relative to the detector axis to an accuracy of 0.3°.

The source chamber is of the same size as the main chamber and a diffusion pump also pumps it. The diffusion is supported by the rotatory pump and cryotrap and can be isolated from the chamber with a quarter swing butterfly valve.
The GaAs sample is mounted so that the surface is in the centre of the main chamber, at the point where the gas beam and the detector axis converge. The sample holder is a self-contained unit which slots into a support fork with pin connectors for the temperature probe and heating element. The sample holder can rotate and allows the angle of incidence of the beam hitting the surface to be changed.
The amount of gas used in these experiments is mixed into the Gas handling apparatus where we control the ratio between the different gases what we want. We control the mix by the pressure.

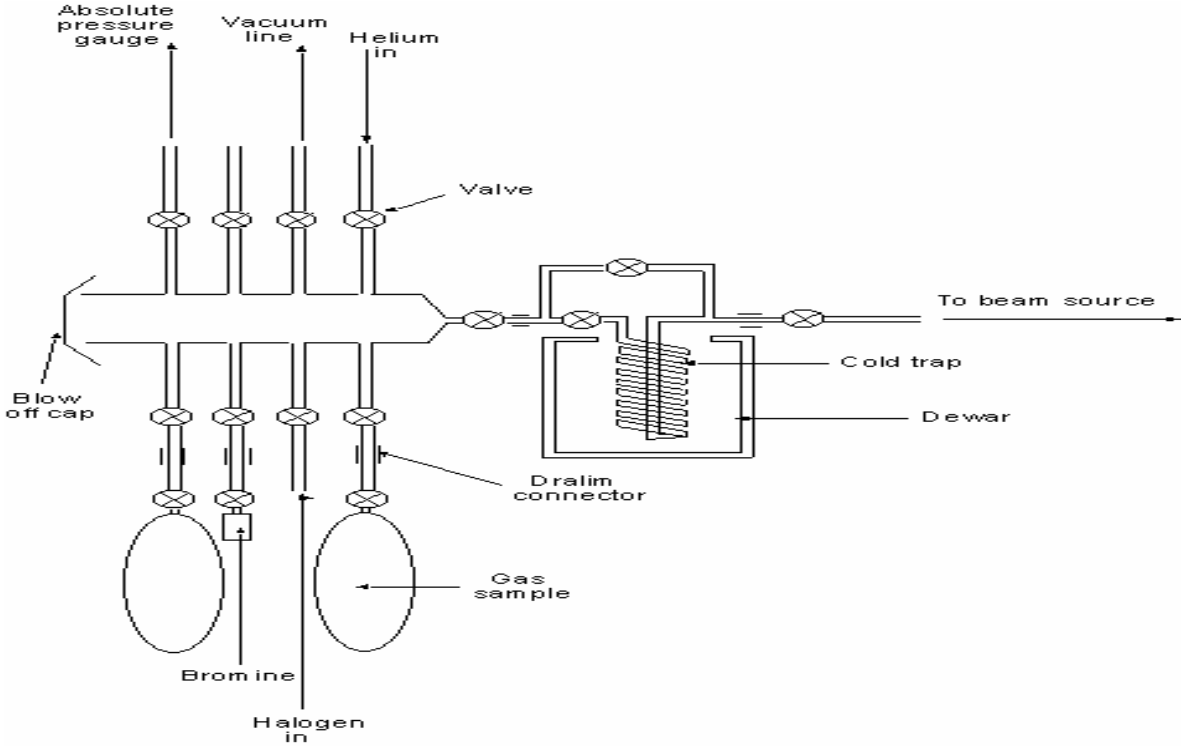

Fig 4. Gas-handling apparatus

Photomultiplier

Photomultiplier tubes (PMTs) convert photons to an electrical signal. They have a high internal gain and are sensitive detectors for low-intensity applications such as fluorescence spectroscopy.
A PMT consists of a photocathode and a series of dynodes in an evacuated glass enclosure. When a photon of sufficient energy strikes the photocathode, it ejects a photoelectron due to the photoelectric effect. The photocathode material is usually a mixture of alkali metals, which make the PMT sensitive to photons throughout the visible region of the electromagnetic spectrum. The photocathode is at a high negative voltage, typically -500 to -1500 volts. The photoelectron is accelerated towards a series of additional electrodes called dynodes. These electrodes are each maintained at successively less negative potentials. Additional electrons are generated at each dynode. This cascading effect creates 10^5 to 10^7 electrons for each photoelectron that is ejected from the photocathode. The amplification depends on the number of dynodes and the accelerating voltage. This amplified electrical signal is collected at an anode at ground potential, which can be measured.

Excimer and dye Lasers

The excimer laser, A in the picture, generates intense pulses (35-70 nJ) of radiation at wavelengths in the UV region of the spectrum, depending of the operating gas mix, by transition from the excited molecules in a high excited state to a low state.

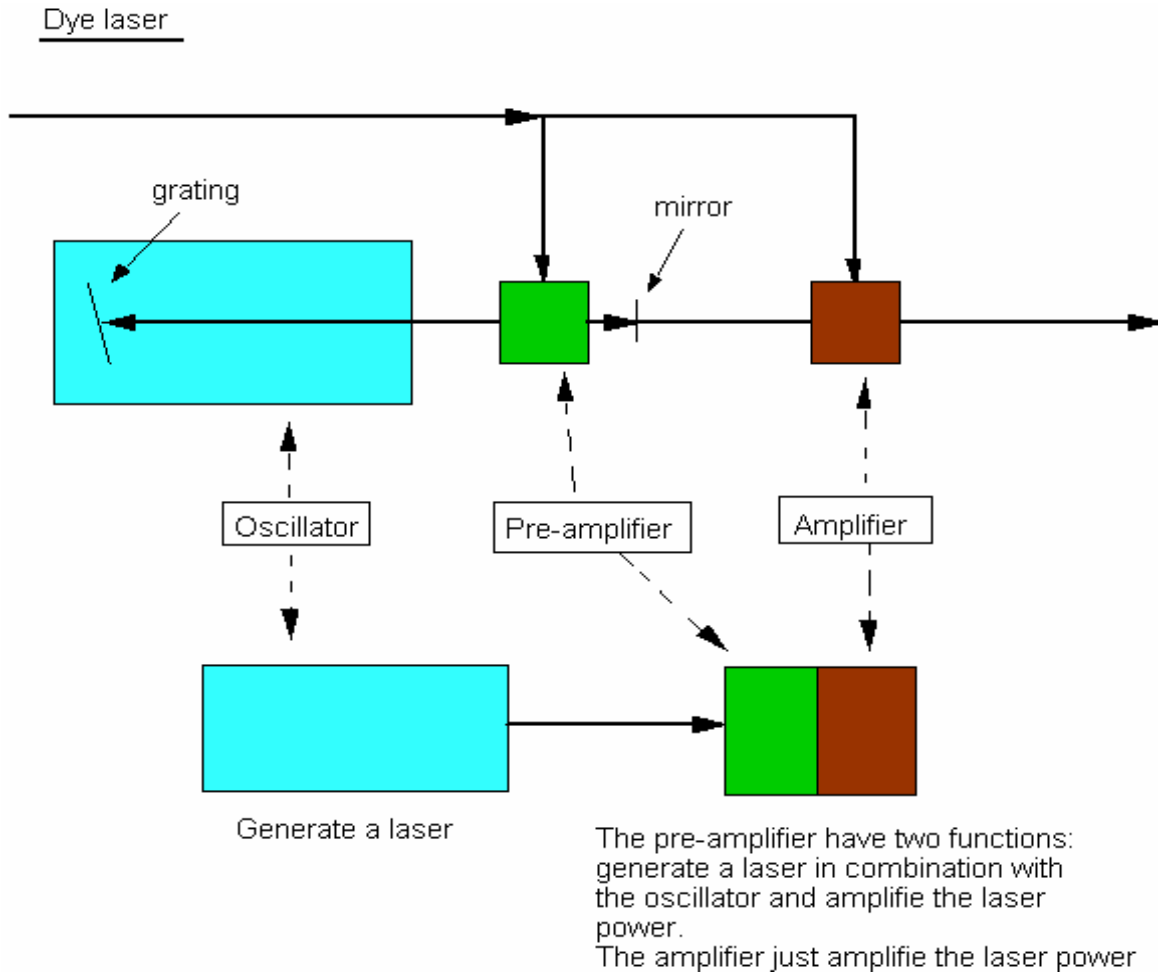

The dye laser, in the picture, is a laser with a tunable wavelength source. The dye laser is pumped by an excimer laser and a weak dye laser is generated in an oscillator, then amplified by the dye laser power amplifiers. Changing the angle of the grating is changed the wavelength of a dye laser.

Quadrupole Mass Spectrometer [8,9,10]

A mass spectrometer is an instrument that produces ions and separates them in the gas phase according to their mass-to-charge ratio (m/q). Today a wide variety of mass spectrometers are available, ranging from benchtop detectors for gas chromatography to room sized instruments.
The principles of operation and the types of experiments that can be performed on these instruments differ greatly.
In this type of mass spectrometer, ions are selected according to their m/q ratio, where m is their mass and q is their electric charge, with no account being taken of the charge sign.

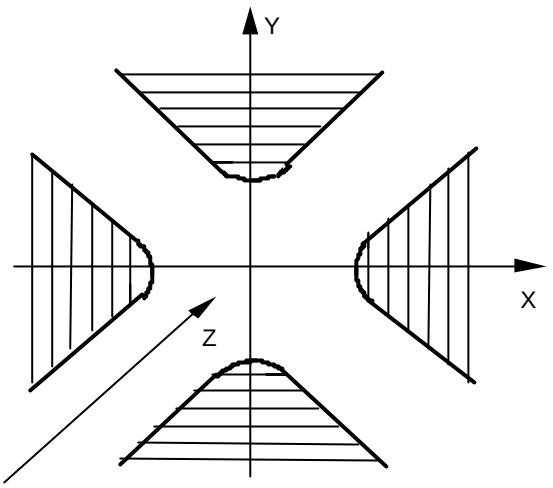

Fig 5. Mechanical structure of a quadrupole filter.

Ideally, it consists of four parallel conductive rods with hyperbolic section to which an electrostatic and a radio frequency (RF) potential are applied simultaneously. Often, in practice, the quadrupole assembly uses four circular section rods.

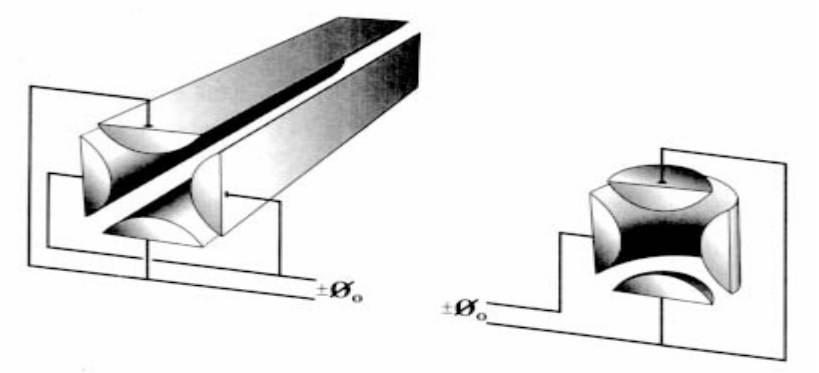

Fig 6 Schematic representation of a quadrupole mass filter and an ion trap, where $\varnothing_0$ is the potential applied to opposite pairs of rods or and cap.

Ions injected into the filter along the Z direction, normal to the plane of Fig., experience a potential field, P, given by

$$P(X,Y,t)=\frac{[U+V\cos(2\pi\times\nu\times t)](X^2-Y^2)}{r_0^2} \quad (53)$$

where r_0 is the shortest distance between the rods and the Z-axis and í is the RF frequency. In other words, the electric potential is

$$U+V\cos(2\pi\times\nu\times t) \quad (54)$$

for the rods lying on the X direction and the opposite sign assumed for the rods on the Y direction. The motion of the ions is described by the Mathieu equations and is rather complicated. Ions may follow stable trajectories and pass through the filter if their displacement from the Z-axis is sufficiently low to avoid collision with the quadrupole

rods. The motion of the ions may be qualitatively understood by considering the separate effect of the positive (X-Z) and negative (Y-Z) planes. In the positive plane ions lie at the bottom of an electrostatic potential well and oscillate under the action of the radiofrequency field. The oscillation amplitude increases with ionic mass, and therefore heavy ions are more likely to be collected by the conducting rods. The function of the X-Z plane is to act on the ion beam like a low-pass mass filter. Using similar arguments one can see that the Y-Z plane works as a high-pass mass filter and the combination of the two planes may be considered as a band-pass mass filter. A more quantitative description of the quadrupole operation can be obtained by means of the stability diagram Fig 7, which represents the field of stability of Mathieu solutions as a function of two parameters:

$$A_u = A_x = -A_y = \frac{8 \times q \times U}{\left[m\left(2\pi \times \nu \times r_0\right)^2\right]} \qquad (55)$$

and

$$Q_u = Q_x = -Q_x = \frac{4 \times q \times V}{\left[m\left(2\pi \times \nu \times r_0\right)^2\right]} \qquad (56)$$

For certain values of A and Q the ionic trajectory may be unstable in the X-Z plane (low pass), in the Y-Z plane (high pass) or in both planes (no transmission). One can also see that there is a well-defined region of stability corresponding to the shadowed area of Fig. 7. In the same figure the line A/Q = const. Is plotted, crossing the stability region at two points that correspond with the lower and upper limits of the filter pass band.

Fig 7

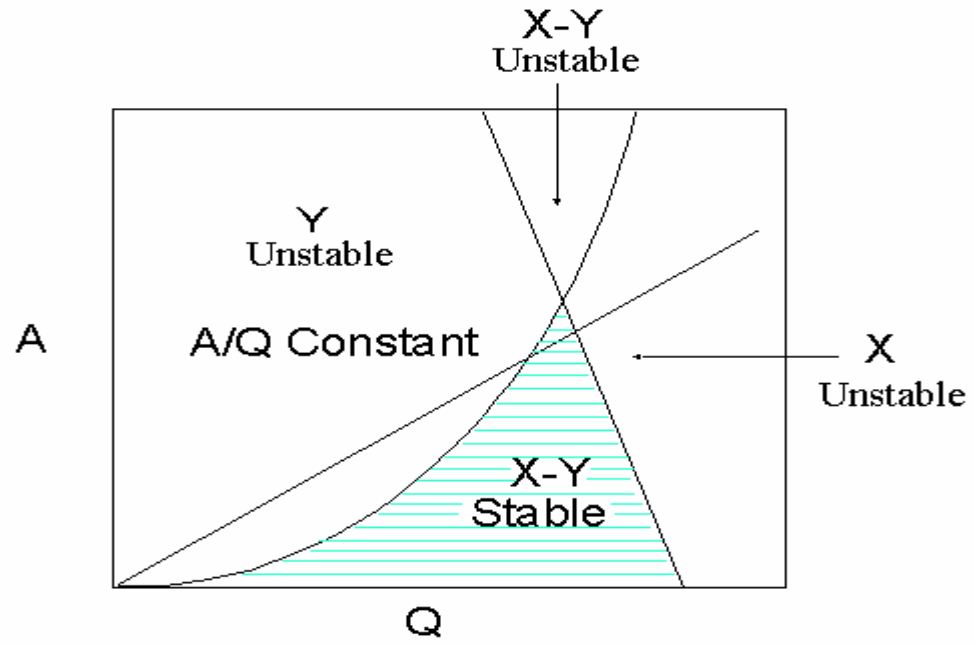

Stability diagram for a quadrupole mass filter. Q and A depend respectively, on the RF and DC components of the quadrupole field. The shared area corresponds to the stabillity condition for the ion motion.

Experimental [11]

Angle-resolved supersonic molecular beam scattering and Time-of-Flight (TOF) analysis are ideal tools to study the dynamics of gas-surface interactions, such as the direct-inelastic scattering and the trapping-desorption. The dynamics of the direct-inelastic scattering and trapping-desorption can be systematically investigated as a function of incident translational energy (E_{inc}), incident angle(θ_i), detection angle (θ_f) and surface temperature(T_S).

When the incident molecules hit a surface, an important fraction of molecules will reflect back to the gas phase by direct-inelastic scattering with essentially zero residence time on the surface. These molecules retain some of their initial translational energy and momentum information, but part of their translational energy can be dissipated into a surface.

The angle- and velocity- resolved measurements of the direct-inelastic scattering can provide information about the dynamics of energy accommodation.

In a highly corrugated surface, such as etched GaAs, the nonconservation of parallel momentum will play a dominant role in the dynamics of reactive gas-surface scattering.

The incident molecules also can be trapped on a surface if the molecules lose enough kinetic energy and these molecules have a finite probability of thermal desorption.

The angular distribution of the desorbed molecules exhibits a $\cos^n(\theta_f)$ dependence (θ_f is the detection angle and n is the energy scaling number mainly ranging from ~0.1 to ~20), which can be used to study the trapping-desorption characteristic and distinguish between molecules that have undergone direct-inelastic scattering and trapping-desorption.

In the experiments here, we carried out a pulsed supersonic molecular beam scattering study of the direct-inelastic scattering and trapping-desorption for Br_2 + GaAs(100) at room temperature. We have measured TOF spectra of scattered Br_2 from GaAs(100) surface as a function of incident translational energy (E_{inc}), incident angle (θ_i) and detection angles(θ_f). The TOF distributions show clearly bimodel consisting of direct-inelastic and trapping-desorption components.

A supersonic molecular beam pulse (~150 μs) is produced from a piezo-electric valve, skimmed and then chopped by a rotating (200 Hz) slotted disc, before passing through a further collimating element, to produce a gas pulse of ~ 35 μs (fwhm) and an angular divergence of ~ 1.5° making a spot size of ~2-3 mm diameter on the target. The housing of a pulsed molecular beam can be rotated around the sample in a plane perpendicular to the sample surface. The pulsed gas molecules hit the surface after a flight of 67 mm from the chopping disc and are scattered towards the floating-potential Brink type ioniser followed by a fast pulse-counting channeltron and a quadrupole mass spectrometer (QMS). The ioniser, in a triply differentially pumped liquid nitrogen cooled chamber, is at a distance of 500 mm from the sample surface. Incident and scattered pulsed molecular beam energies are determined from TOF measurements. The TOF spectra were corrected for the ion flight time through the QMS.

Results

Mathematical method for Time-of-Flight waveform analyses

Fig.1(a) illustrates typical number density TOF spectrum of scattered Br_2 from GaAs(100) surface at 25°C for an incident translational energy E_{inc} = 85.45 kJmol^{-1} at an incident angle, θ_i = 80°, and detection angle, θ_f = 60°. This TOF spectrum displays clearly that it is composed of a narrower fast peak that is superimposed on the leading edge of the second slower and broader peak. The fast narrow peak can be assigned to the direct-inelastic scattering. In contrast, the slow broader peak which fully trapped onto the surface and subsequently desorbs is assigned to the trapping-desorption.

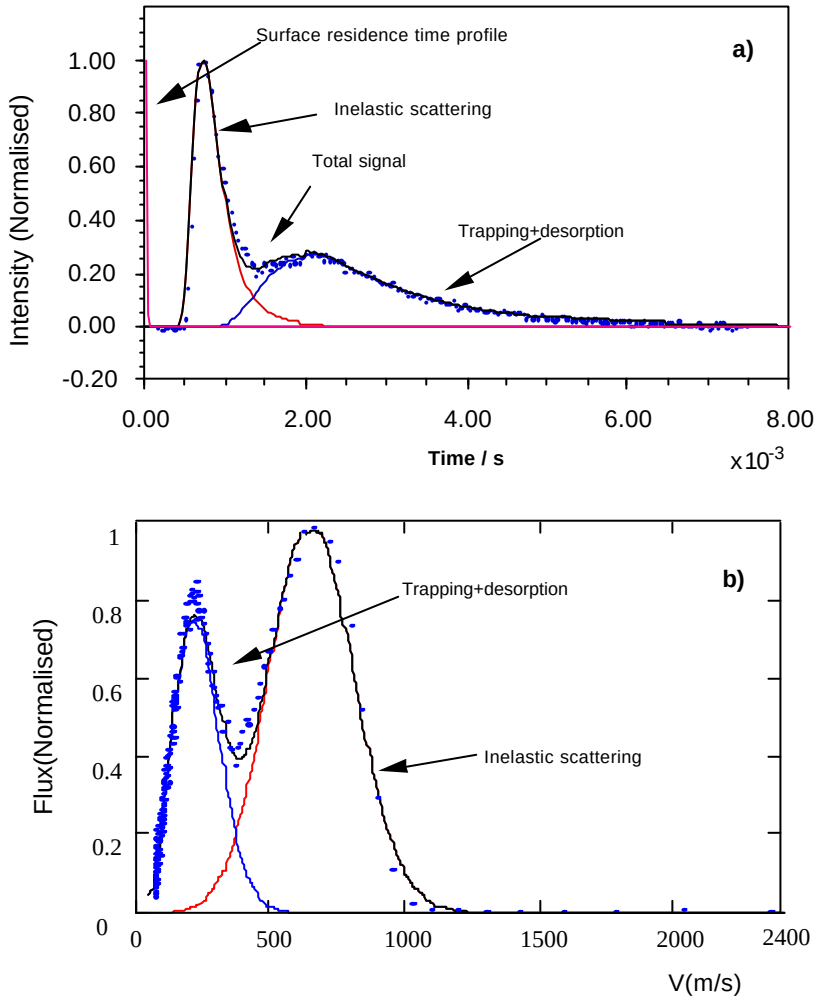

Fig.1 a), TOF intensity distribution of Br_2 scattered from GaAs(100) surface. The lines are backfits to Eq(2). b), Velocity flux distribution of Br_2 converted from the same TOF intensity distribution from a). The lines are backfits to Eq(3). The experimental conditions: E_{inc} =85.45 kJ/mol, θ_i =80°, θ_f =60°, T_s =25°C .

The contribution from the direct-inelastic and trapping-desorption components can be found by fitting the observed TOF waveform to a two component model, made up from a modified gaussian and a Maxwell-Boltzmann distribution at the surface temperature T_S:

$$F(v,vi) = A\left(F_{di}(v,vi) + BF_{td}(v)\right) \quad (57)$$

Where $F_{di}(v,v_i)$ and $F_{td}(v)$ are the flux of direct-inelastic scattering and trapping-desorption components; A and B are weights for the total and trapping-desorption fluxes, respectively. v_i indicates the direct-inelastic peak position. Converting Eq (57) to number density and time:

$$T(t) = A\left[\frac{s^3}{t^4}\exp\left[-\left(\frac{s}{\alpha}\left(\frac{1}{t}-\frac{1}{t_i}\right)\right)^2\right] + B\left(\int_0^t \exp\left(-\frac{t_d}{\tau_d}\right)T_{MB}(t-t_d)dt_d\right)\right] \quad (58)$$

where s is the flight distance and α is the width of the direct-inelastic peak and τ_d is the surface residence time of trapping-desorption species on the surface which we will describe details later in this paper. Eq(58) is true providing that the gas pulse can be treated as a δ function, which can be met in our experimental conditions. At short surface residence times, the measured TOF of trapping-desorption component approaches closely to that expected from a Maxwell-Boltzmann distribution at the surface temperature $T_{MB}(t)$. At long surface residence times, the TOF of trapping-desorption deviates from a Maxwell-Boltzmann distribution with a shift of the peak and long tail.

The lines in Fig.1(a) are least-squares best fits to Eq.(58). In order to obtain angular distributions, the flux of the scattered Br_2 is needed. The intensity-time (number density) frame has to be changed to flux-velocity frame. The following equation was used to transfer from intensity-time distribution to flux-velocity distribution:

$$F(v) = T\left(\frac{s}{v}\right)\frac{s}{v} \quad (59)$$

Fig.1(b) displays the velocity-flux distribution transferred from its TOF number density distribution(Fig.1(a)). Integration of the two peaks in Eq. (59) provides the relative contributions of the direct-inelastic scattering and trapping-desorption components to the total observed signals. The ratio of the trapping-desorption part to the total signals can be used as relative trapping-desorption probability.

Incident translational energy dependence

Fig.2 shows the number intensity TOF distributions of scattered Br_2 from GaAs(100) at the incident angle θ_i = 80°, detection angle θ_f = 60° for various initial translational

energies (E_{inc}). All the measured number density distributions of Br_2 molecules arriving at QMS are normalised and GaAs(100) surface temperature was 25°C.
The direct-inelastic components increase with the initial translational energy. The solid lines through the data represent the sum of the direct-inelastic and trapping-desorption components. The trapping-desorption part was fitted to Maxwell-Boltzmann distributions with its surface residence time applied. The increase of the ratio of the direct-inelastic component to the trapping-desorption means that a molecule is less likely to be trapped on the surface when the initial translational energy increases.

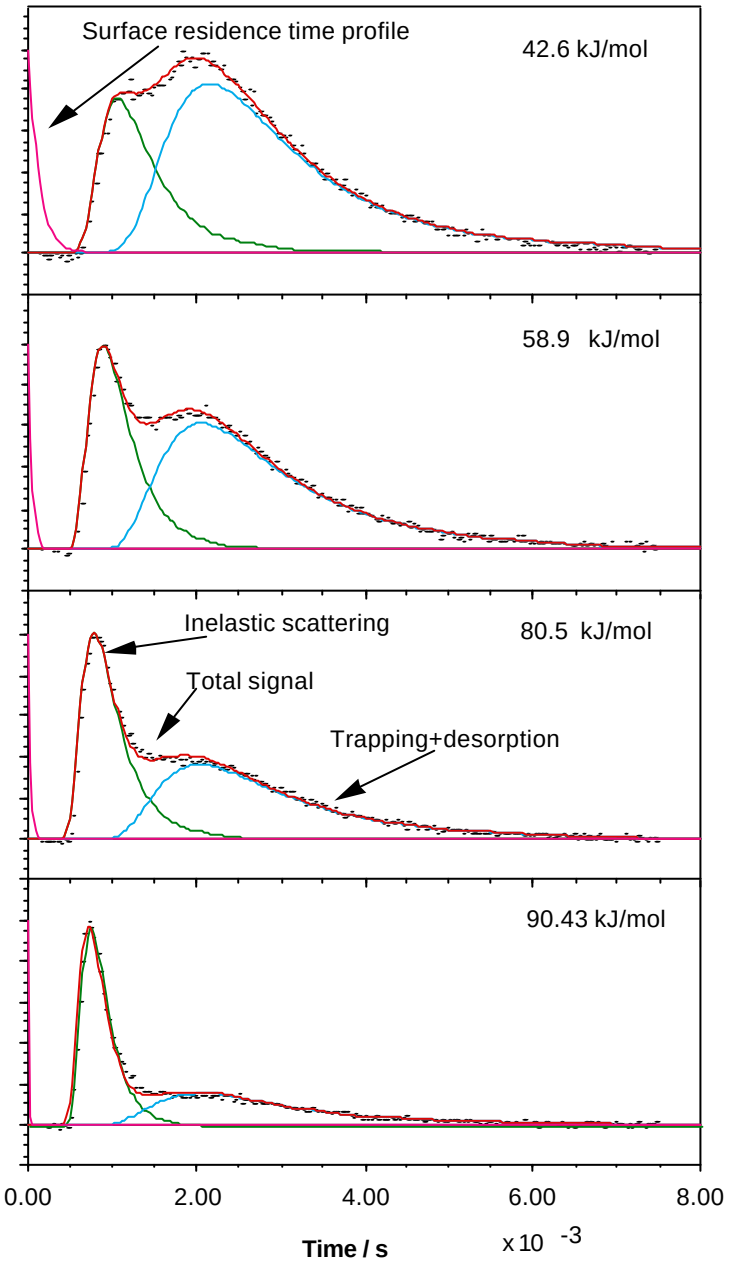

Fig.2 TOF spectra of Br_2 scattered from GaAs(100) surface at temperature of 25°C for various incident translational energies. The incident angle was 80°,the detection angle was 60°.

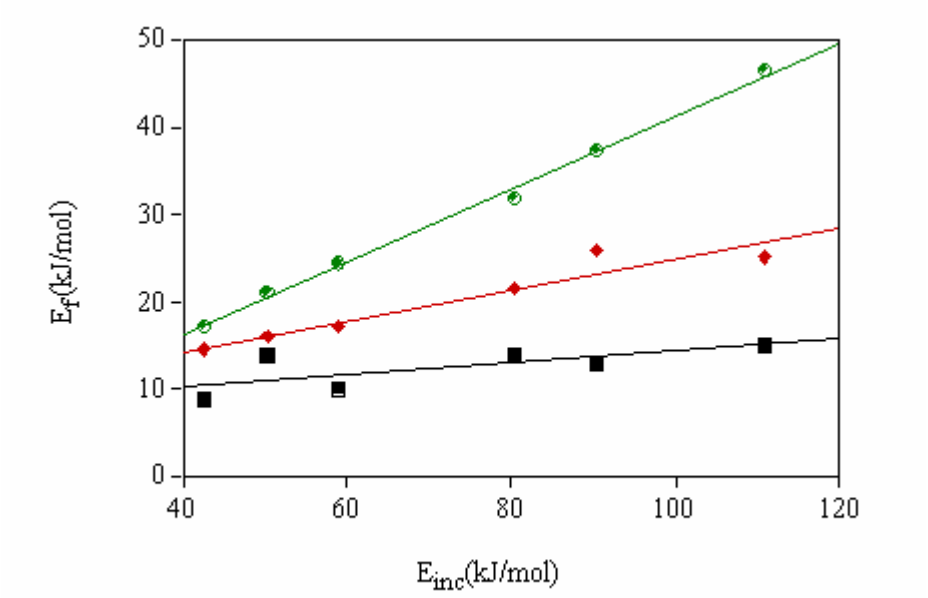

Fig.3. The final output translational energy E_f of the direct-inelastically scattered Br_2 from GaAs (100) surface at temperature of 25 ^{o} C for their various initial incident translational energy E_{inc}. The detection angle was 60^o. The filled circles, diamonds and squares represent the incident angles of 80^o, 60^o and 30^o, respectively.

Fig.3 illustrates the final exit average translational energy (E_f) of direct-inelastic scattering of Br_2 with the initial incident translational energy (E_{inc}) at incident angles of 30°, 60° and 80°. Two main features can be observed in this graph: 1) E_f increases with increase of incident translational energy (E_{inc}). The correlation between E_f and E_{inc} displays a good linear relationship at fixed incident and detection angle. 2) E_f and the change of E_f respect to E_{inc} increase with increase of incident angle. A larger fraction of E_{inc} is exchanged at more normal angles of incidence. This behaviour was attributed to more efficient coupling of translational energy to surface phonon as incident angle is more normal to the surface. For a conditions of E_{inc}=110.9 kJ/mol, è$_f$=60° and GaAs(100) surface temperature at 25°C, about 42% of the incident energy of Br_2 transfers into a direct-inelastic energy at è$_i$=80°, but only 13.7% of E_{inc} transfers to E_f at è$_i$=30°.

Polar angular distribution

The polar angular distributions of the total counts, direct-inelastic scattering and trapping-desorption of Br_2 for è$_i$=30°, è$_i$=60° and è$_i$=80° have also been shown in Fig.6.

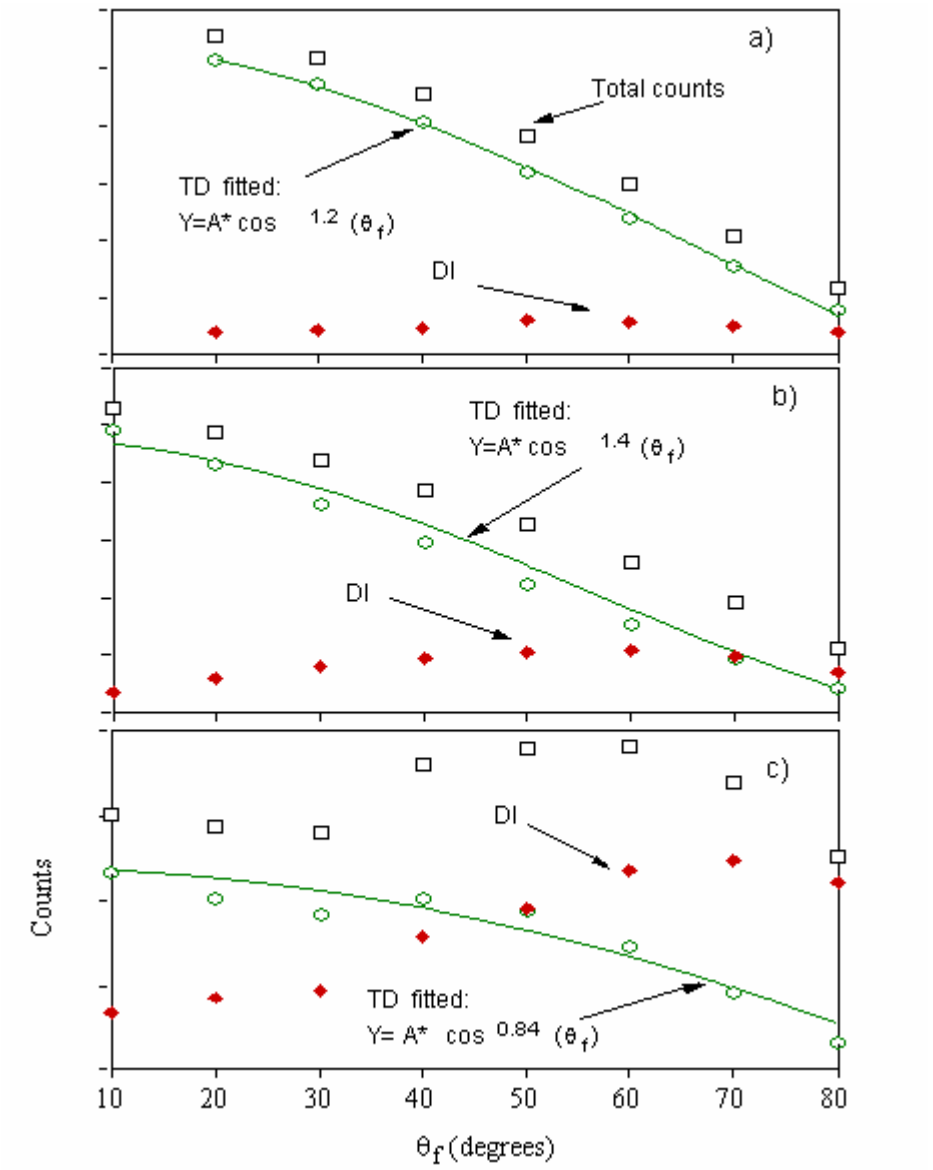

Fig 6. The number density angular distributions of Br_2 at T_s=25 ^oC of the total, trapping desorption (TD) and direct-inelastic (DI) for a)θ_i=30 ^oC, b)θ_i=60 ^oC and c)θ_i=80 ^oC to the surface normal, respectively, with E_{inc}=91.45 kJ/mol

From Fig.6 we found that all polar angular distributions of the trapping-desorption are close to cosine distribution. The angular distributions of the direct-inelastic scattering are close to their specular angles. Fig.7 shows the angular distributions of Br_2 for three different incident translational energies (42.34, 60.24, and 91.45 kJ/mol, respectively) at è$_i$=60°.

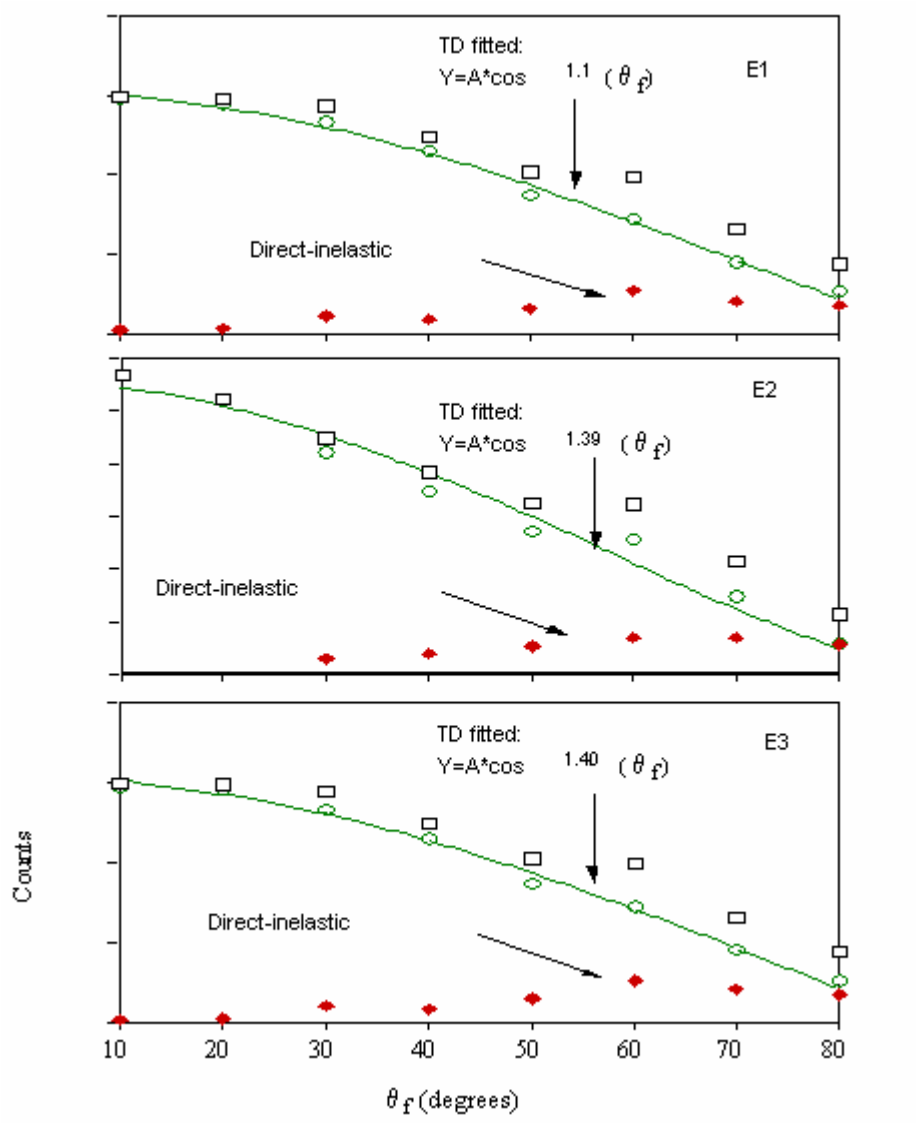

Fig 7. The angular distributions of Br_2 for the three different initial translational energies, E_1=42.34 kJ/mol, E_2=60.24 kJ/mol and E_3=91.45 kJ/mol. θ_i=25°C. The squares are total intensity, the circles and filled diamonds are the trapping-desorption and direct-inelastic scattering, respectively.

It clearly shows that all the direct-inelastic components peaked near the specular angle although the E_{inc} has been changed from 42.34 kJ/mol to 91.45 kJ/mol. The trapping-desorption components are near cosine distribution, which represents a Maxwell-Boltzmann behaviour. From these angular distribution, it clearly indicates that E_{inc} has very little affect on the trapping-desorption and direct-inelastic scattering features. These results show that trapping-desorption components follows Knudsen law with cosine distribution, independent of è$_i$ and E_{inc}, while direct-inelastic scattering is isotropic, depends on the incident angle and a maximum peak is near its specular angle.

Incident angle distribution

The initial incident translational energy can be divided into perpendicular energy (also called normal energy: $E_{inc}\cos^2(\theta_i)$) and parallel energy ($E_{inc}\sin^2(\theta_i)$). By change of incident angle, we can examine which part of incident momentum will have more influence on scattering features.

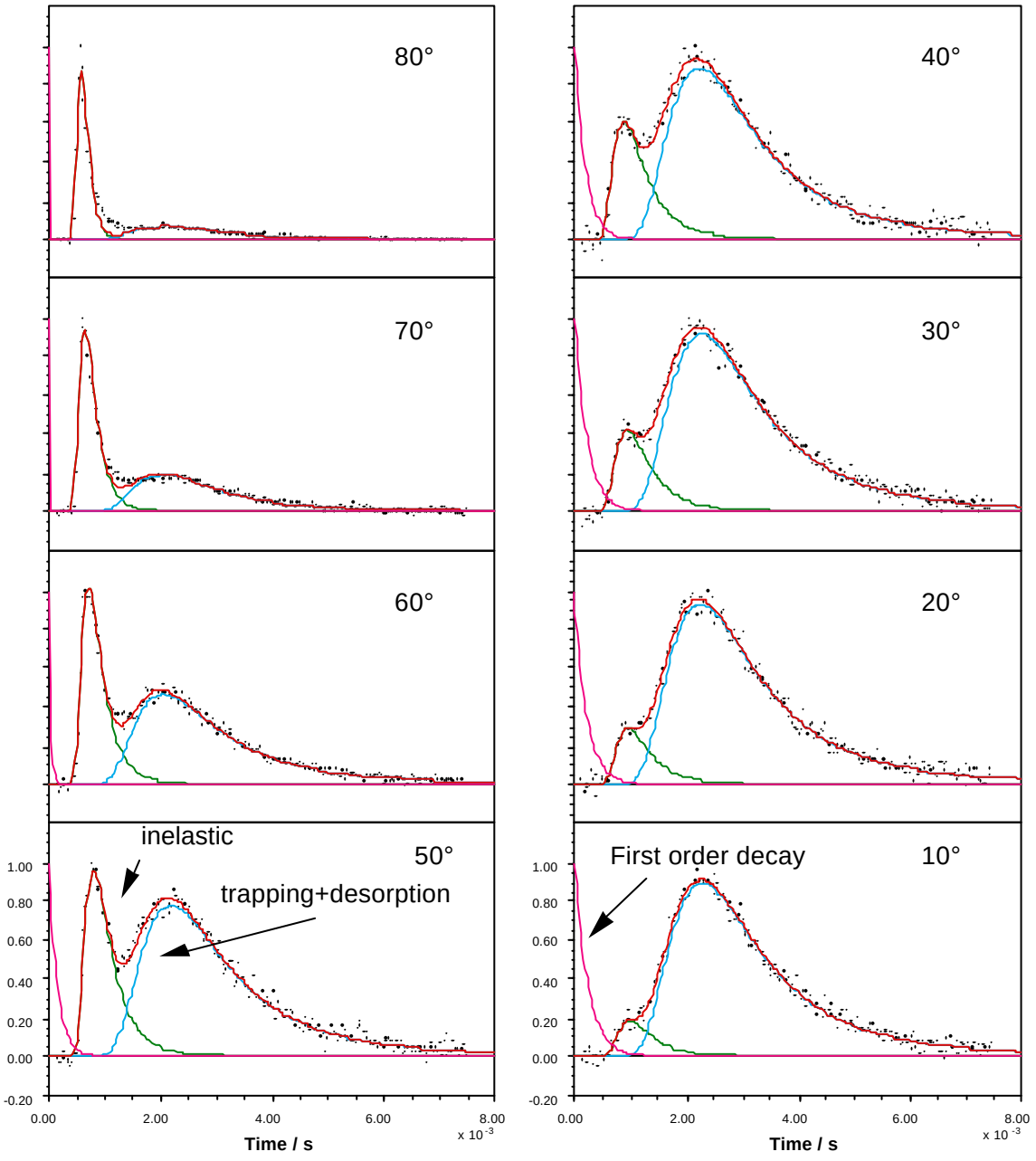

Fig.8 TOF distribution of inelastic and trapping+desorption scattering of Br_2 with various incident angles. The detection angle was 80°; the initial translational energy of the supersonic molecular beam of Br_2 was 91.45 kJ/mol and the GaAs(100) surface temperature was 25 °C.

Fig8. shows TOF intensity distributions of various incident angle for E_{inc} = 91.45 kJ/mol, è$_f$=80°, and T_S=25°C. As è$_i$ decrease, the direct-inelastic component falls off, and trapping-desorption component arises.

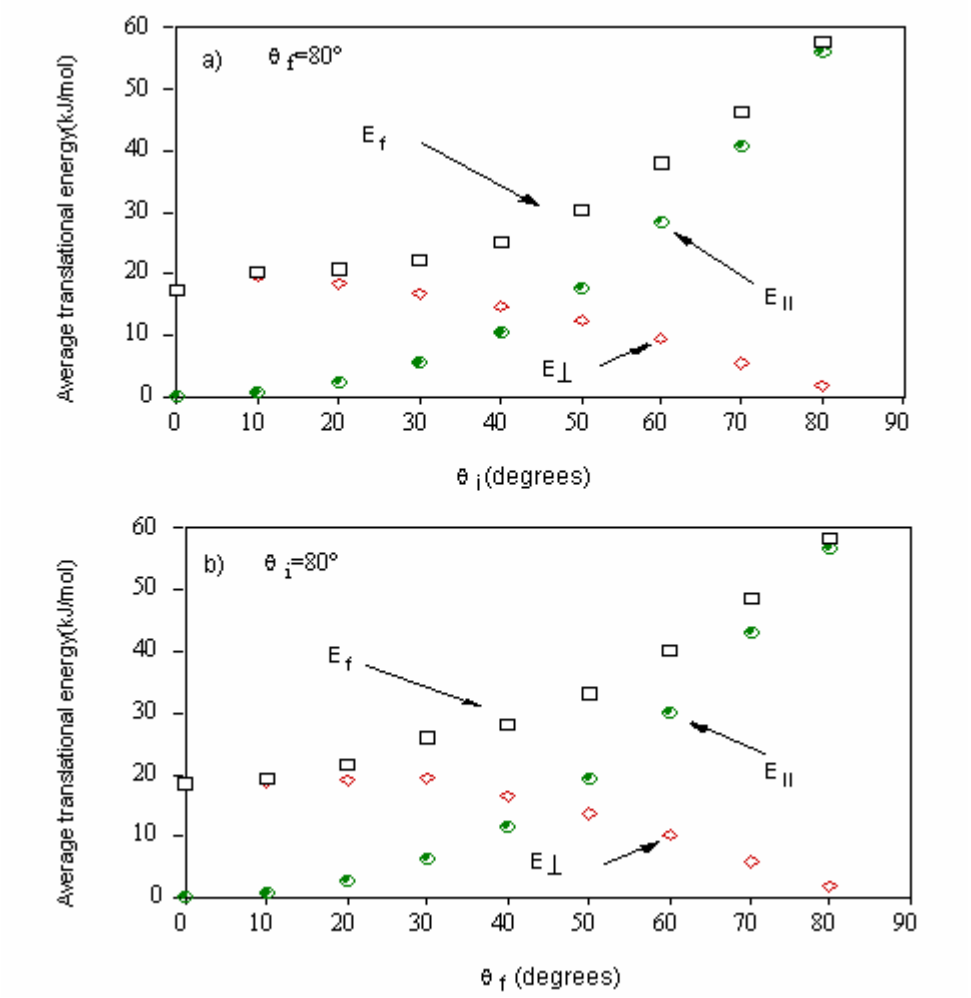

Fig 10 Comparison of the angular dependence of the output energy (final, perpendicular and parallel) of inelastically scattered Br_2 for a) the fixed detection angle θ_f = 80º and b) the fixed incident angle θ_i = 80°. The initial translational energy was 91.45 kJ/mol and the surface temperature was 25ºC

Fig.10 shows two important features: 1) incident and detection angular dependence of E_f, E and $E_{||}$ are same. 2), At small angles (è$_i$ or è$_f$<30°), E_f change is very small and is mainly attributed to the perpendicular energy(E). At large angle (è$_i$ or è$_f$>40°), the total output energy increase dramatically, in which E_f was mainly attributed to $E_{||}$.

Laser-Induced Fluorescence [5]

Laser-induced fluorescence (LIF) is the optical emission from molecules that have been excited to higher energy levels by absorption of electromagnetic radiation.
In (LIF), a sample absorbs electromagnetic radiation from a laser and some of its molecules are excited to higher energy levels. Fluorescence is emitted at wavelengths longer than the exciting radiation. Both the absorbed and emitted wavelengths are characteristic of a given molecule.

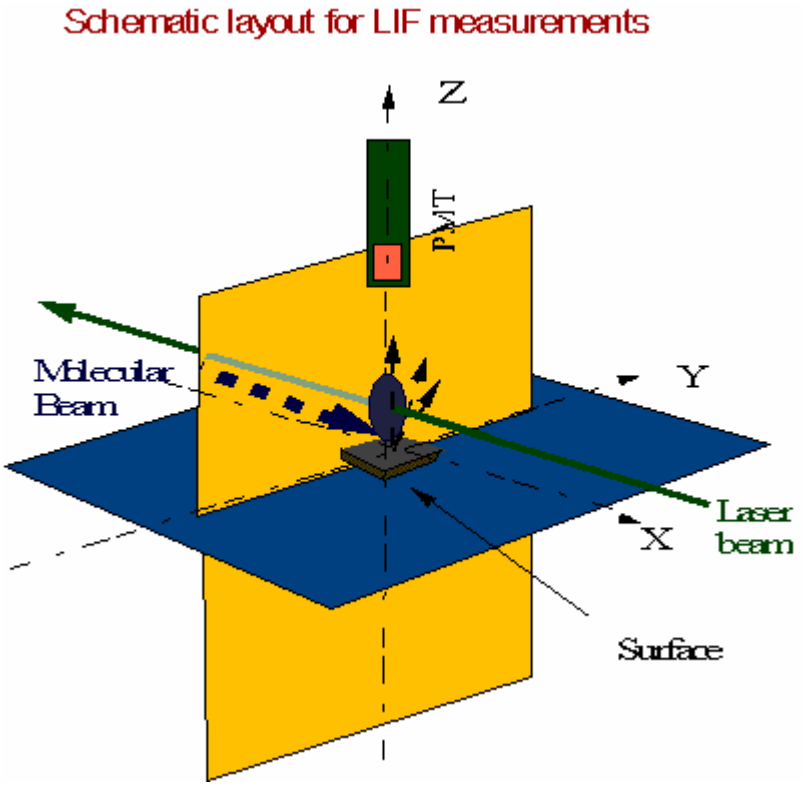

The molecules internal energy distributions (electronic, vibrational, and rotational) can be determined. Therefore energy information before and after scattering of a molecule from a surface can be obtained.
In addition to obtaining internal energy information, the angular distribution can be determined by turning the sample surface, thus scattered molecules are excited by the laser and produce fluorescence detected by a Photomultiplier.
Because the emitted wavelength is different to the exciting wavelength, fluorescence detection is very sensitive relative to absorption measurements. In some cases LIF sensitivities approach the detection of a single atom or molecule, also for molecules that can be resonant excited, LIF provides selective excitation of the sample to avoid interferences.

The LIF spectrum has two forms: Low resolution spectra and high-resolution spectra.

Low-resolution spectra

The peak signal height of each vibration bandhead is measured, divided by the Fanck-Condon factor for the absorption and further divided by the laser photon flux at the

excitation wavelength (measured relative to the peak flux of the dye range). If the intensity of emission for any upper vibrational state is assumed to be constant, this directly yields the relative vibrational populations if the variation of emission probability with transitions frequency is assumed to be negligible.
T_{vib}, characteristic vibrational temperature is obtained from the assumption that the relative vibrational populations follow the Boltzmann equation:

$$N(v'') \propto \exp(-E_{vib}/kT_{vib})$$

Where $E \cong (v'' + \frac{1}{2})\omega_e hc$ to a first approximation

Hence: $\ln(N(v'')) = -(v'' + \frac{1}{2})\omega_e hc/kT_{vib}$

Therefore, a plot of $\ln(N(v''))$ vs. $(v'' + \frac{1}{2})$ yields a gradient of $\omega_e hc/kT_{vib}$, giving a value for T_{vib}.

High-resolution spectra

Well isolated P and R branch rotational pairs occur for high rotational quantum (J) numbers for same vibrational bands which are sufficiently separated to prevent overlap at these high J values.
In scattering experiments the molecules are not in thermal equilibrium so they are not characterized by T_{vib} and T_{rot}. The LIF spectra are used to find the initial lower state vibrational and rotational population.

Energy gap, wavelength and frequency of transitions

To deduce the energy difference between defined vibrotational states in the ground and excited electronic states the energies of the electronic, vibrational and rotational modes of the molecules must be considered

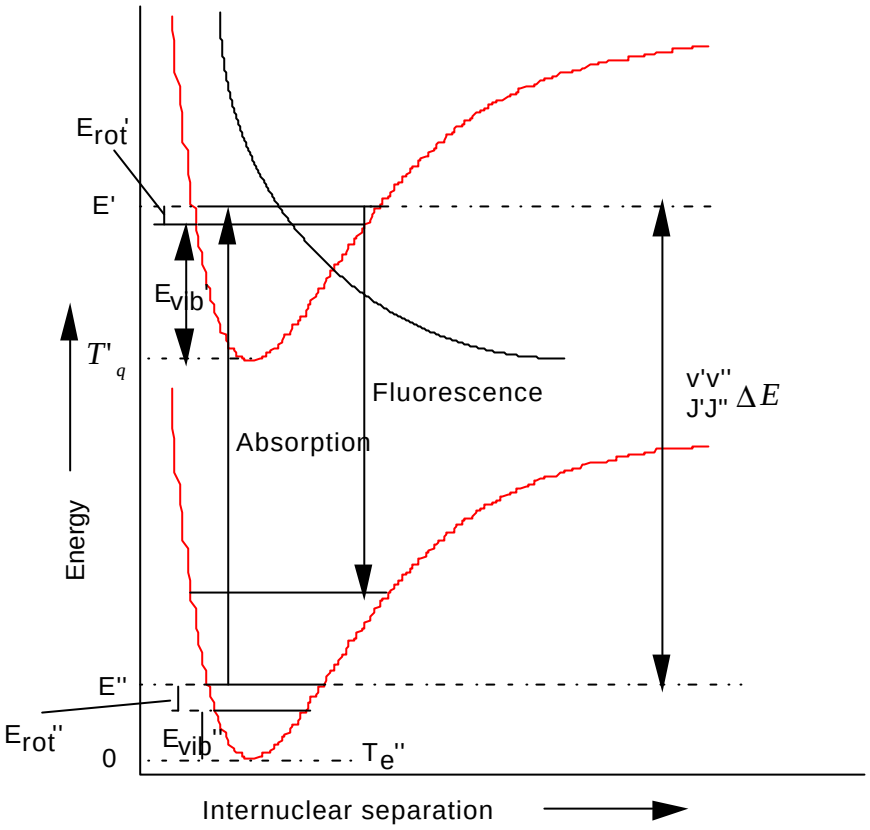

Typical form of the potential energy curves for the ground and excited electronic states of a diatomic molecule (the term symbols are applicable to Br_2).

All the energies are referred to the minimum of the ground state potential; so $T_e'' = 0.0$
The vibrational energy, E_{vib}, for any molecule with vibrational quantum number v, referred to the minimum of its potential energy curves is approximately given by the eq.(39) and the rotational energy, E_{rot}, of a molecule with rotational quantum number J, referred to the J = 0 level for any vibrational level, is given by the eq.(25) being $E_{vib}+E_{rot}$ given in the eq (49).
Hence $E = T_e + E_{vib} + E_{rot}$ and the energy difference between defined vibrotational states in the ground and excited electronic states is given by

$$\Delta E = E' - E'' \qquad (60)$$

Then substituting and converting units, we have the frequency of the transition, n, in Hertz

$$\nu = {}^{\upsilon',\upsilon''}_{J',J''}\Delta E \cdot c \qquad (61)$$

where c is the velocity of light in $cm.s^{-1}$.

Intensity of emission, (I_{pc})

The emission intensity in $J\ s^{-1}$ from a given J′ state to any allowed J′′ state is given, for an upper state rotational population, F(υ′,J′), as:

$$ {}^{\upsilon'\upsilon''}_{J'J''}I_{em} = \frac{K_1 \cdot \nu^4 \cdot S_e(J',J'') \cdot F(\upsilon',J')}{(2J'+1)} \qquad (62) $$

Where K_1 is a proportionality constant and $S_e(J',J'')$ is the Honl-London factor for the rotational transition. However the detector signal is photon flux, so we must divide by hν dividing:

$$ {}^{\upsilon'\upsilon''}_{J'J''}I_{pc} = \frac{K_2 \cdot \nu^3 \cdot S_e(J',J'') \cdot F(\upsilon',J')}{(2J'+1)} \qquad (63) $$

The emission also involves a transition in vibrational quantum number, so the Franck-Condon factor, $q_e(\upsilon',\upsilon'')$ must be also be included:

$$ {}^{\upsilon'\upsilon''}_{J'J''}I_{pc} = \frac{K_3 \cdot \nu^3 \cdot S_e(J',J'') \cdot q_e(\upsilon',\upsilon'') \cdot F(\upsilon',J')}{(2J'+1)} \qquad (64) $$

The transitions also involve a change in electronic state. The electronic transition moment is assumed to be independent of vibrational and rotational quantum number, being a constant included in the term K_3.
The experimental LIF spectrum also depends on the spectral efficiency of the detector, which is a function of wavelength, $D(\lambda_{em})$.
Then, in general, the relative photon count rate, $\langle I_{pc} \rangle$, is a summation of the above equation over all allowed values of v'' and J'' in emission, without the proportionality constant:

$$ \langle I_{pc} \rangle = \sum_{\substack{\text{all-}\upsilon'' \\ \text{all-allowed-}J''}} \frac{\nu^3 \cdot S_e(J',J'') \cdot q_e(\upsilon',\upsilon'') \cdot F(\upsilon',J') \cdot D(\lambda_{em})}{(2J'+1)} \qquad (65) $$

Population, F(u℄,J℄)

The population, $F(\upsilon',J')$ is determined by the absorption process, which occur from the ground state to this state. This population is proportional to the laser photon flux at the absorbing wavelength, $\phi(\lambda_{abs})$, the relative population of the ground state, $F_{ini}(\upsilon'',J'')$, the Franck-Condon factor for the absorption, $q_a(\nu'',\nu')$, and the Honl-London factor for the rotational absorption, $S_a(J'',J')$.
Then:

$$ {}^{\upsilon''\upsilon'}_{J''J'}I_{flux} = \frac{K \cdot S_a(J'',J') \cdot q_e(\upsilon'',\upsilon') \cdot F_{ini}(\upsilon'',J'') \cdot \phi(\lambda_{abs})}{(2J'+1)} \qquad (66) $$

The electronic transition probability is assumed to be a constant, independent of the vibrational and rotational quantum numbers, and hence is included in the factor K.

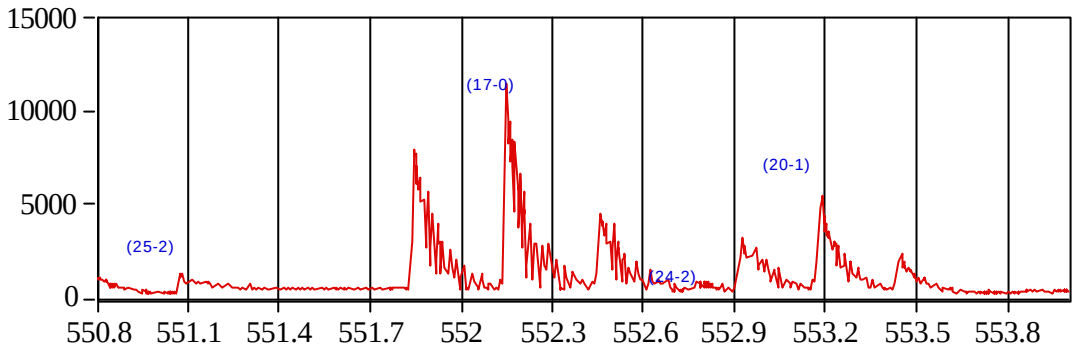

Fig 1 shows a typical LIF spectrum for Br_2. The different peaks are the transitions of LIF between a vibrational level, $\upsilon''=0$ of the ground electronic level, X $^1\Sigma_g^+$ to vibrational level, $\upsilon'=17$ of the excited electronic level, B $^3\Pi_{ou}^+$, in the case of the (17-0) transition. As we can see, for example (17-0) transition, we have three large peaks. Each one is due to a different isotope mixture of Br_2, $^{79}Br^{79}Br$, $^{79}Br^{81}Br$ and $^{81}Br^{81}Br$. The isotope abundance ratio is 1:2:1. We are interested in the $^{79}Br^{81}Br$, the biggest one in this case. If we have a look at of a particular vibrational level, we see, fig 2:

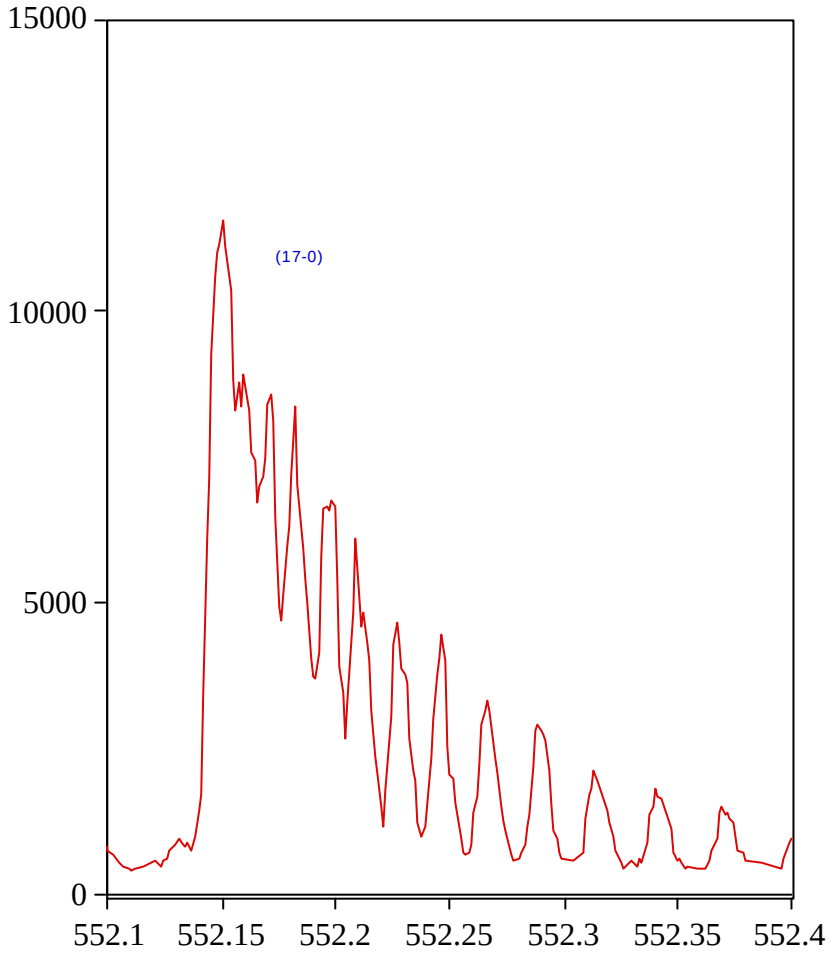

This rotationally resolved spectrum is for the transition from the vibrational level, $\upsilon''=0$ into a ground electronic level, X $^1\Sigma_g^+$ to the vibrational level, $\upsilon'=17$, into an excited electronic level, B $^3\Pi_{ou}^+$, of Br_2. The x-axis is the wavelength, λ, and the y-axis is the intensity of the fluorescence. In this picture we can see with more detail the different rotational level associated with a particular vibrational level.

Bibliography

[1] Fundamentals of molecular spectroscopy
Colin N. Banwell and Elaine M. McCash
McGraw-Hill 4th Ed. 1994

[2] Physical Chemistry
P. W. Atkins
Oxford University Press 1998

[3] Molecular Spectroscopy
Jeanne L. McHale
Prentice Hall 1999

[4] Spectra of Diatomic Molecules
Gerhard Herzberg, F. R. S.
2nd Ed. Litton Educational Publishing 1950

[5] S. J. Bullman
PhD Thesis. University of Manchester 1982

[6] Jonathan Essex-Lopresti
PhD. Thesis.University of Manchester 1999

[7] Basic Vacuum Technology
A. Chambers, S. K. Fitch and B. S. Halliday
IOP Publishing Ltd.1989

[8] Atomic and molecular beam methods
Chapter 8 by D. Bassi
Edited by Giancinto Scoles
Oxford University Press 1988

[9] http://www.ms.mc.vanderbilt.edu/tutorials/ms/2.htm - 2-3-2

[10] http://www.chem.qmw.ac.uk/surfaces/scc/scat6_3.htm

[11] Weiji Jia, Jose L. Ibarra, J. C. Whitehead, Peter A. Gorry
To be published